Carbon 218 (2024) 118742

Contents lists available at ScienceDirect

Carbon

journal homepage: www.elsevier.com/locate/carbon

Synergistic lubrication mechanism of nanodiamonds with organic friction modifier

A.K. Piya [a,b,*], L. Yang [a], A. Al Sheikh Omar [a], N. Emami [b], A. Morina [a]

[a] School of Mechanical Engineering, University of Leeds, LS2 9JT, Leeds, UK
[b] Division of Machine Elements, Luleå University of Technology, 971 87, Luleå, Sweden

ARTICLE INFO

Keywords:
Organic friction modifier
Nanodiamond
Friction
Wear
Tribofilm

ABSTRACT

Nanoparticles and organic friction modifiers (OFMs) as lubricant additives have shown great potential in friction and wear reduction by forming tribofilms which prevent direct contact at the sliding interface. Potential mechanisms for the formation of these tribofilms remain poorly understood, limiting the ability to optimise the performance of the entire tribosystem. Incorporation of nanoparticles and OFM together in a lubricant could provide a unique solution to enhance frictional and wear properties. In this study, Nanodiamonds (NDs) and Glycerol Monooleate (GMO) have been added to a PAO base oil containing low concentration of Zinc dialkyl dithio-phosphate (ZDDP) to produce a novel lubricant combination that significantly reduces coefficient of friction (COF) and wear. Experimental studies showed that NDs reacted with additives present in the lubricant combination to expedite tribofilm formation. Friction reduction performance can be attributed to the encapsulation of carboxylated NDs due to tribochemical interaction with GMO, their mechanical interlocking in the tribofilm and polishing effect of NDs. The visible presence of NDs in tribofilms and the formation of a thicker tribofilm layer with NDs have been corroborated for the first time in this study. Synergy achieved among NDs, GMO, and low concentration ZDDP to formulate a novel environmentally friendly lubricant with advanced tribological performance has been shown, providing a great potential to develop sustainable tribological solutions for a wide variety of engineering applications.

1. Introduction

Friction and wear govern the energy efficiency and service life of moving components. A striking amount of energy is consumed in overcoming friction and wear across various industries [1,2]. Friction reduction is the foremost strategy to enhance energy efficiency often achieved by introducing lubricating oil that forms a protective barrier between rubbing surfaces [3]. Enhancing lubricants' properties and their interactions with the contacting surfaces to improve tribological performance is an impactful solution for global energy challenges. Currently, researchers are focusing on developing new emerging technologies to substitute conventional lubricants and additives containing environmentally hazardous elements with eco-friendly compounds [4–8]. Among organic friction modifiers, GMO is well documented to significantly improve tribological performance by forming protective films or self-assembled structures on the surfaces through its functional groups, which enable systematic and close adsorption on iron surfaces [9,10]. Zinc dialkyl dithiophosphate (ZDDP), on the other hand, is a prominent Phosphorus (P) and Sulphur(S) based additive that provides anti-oxidant and anti-wear performance for engine and transmission system. Interactions between ZDDP and various FMs affected the formation rate and chemical composition of ZDDP-derived tribofilm [9,10]. Even though incorporating GMO with different lubricant combinations showed promising results, certain drawbacks persisted [9,11]. It has been demonstrated that the presence of GMO and ZDDP in a PAO base oil lubricant combination reduces ZDDP tribofilm thickness. However, friction reduction tends to be limited, and the effect of ZDDP on frictional performance depends on surface chemistry and concentration [12,13]. In addition, the presence of ZDDP might have an antagonistic effect by increasing the coefficient of friction, particularly at elevated temperatures [14]. Hence, it is worth investigating the potential effect of lubricant combination of PAO base oil with GMO and ZDDP in steel tribopair for engineering applications.

To comply with current environmental legislation, it is important to reduce the amount of S and P concentration in current lubricant combinations [15]. Hence, to achieve the goal, environmentally friendly alternatives such as nanoparticles can be an option. Commonly used nanoparticles in lubricant industries are layered molybdenum disulfide

* Corresponding author. School of Mechanical Engineering, University of Leeds, LS2 9JT, Leeds, UK.
E-mail address: mnakp@leeds.ac.uk (A.K. Piya).

https://doi.org/10.1016/j.carbon.2023.118742
Received 18 August 2023; Received in revised form 3 December 2023; Accepted 14 December 2023
Available online 19 December 2023

MoS_2, graphite, hexagonal boron nitride (h-BN) and other metal nanoparticles like Zn, Al, Cu, Ti, Fe etc. [16]. However, these nanoadditives such as MoS_2 or graphite readily oxidise under heavy load, reducing their lubricating effect [17]. Due to high compatibility and substantially reduced environmental impact, ultrafine carbon-based additives such as NDs are considered a promising solution in nanomaterial lubricant additive studies [18]. NDs are ultrafine particles of diamonds with higher surface area; they are extremely hard and can provide excellent wear resistance to surfaces [19]. In addition, NDs retain superior chemical stability (i.e. oxidation resistance), outstanding thermal stability and excellent mechanical properties [20]. NDs with diameters smaller than 50 nm have demonstrated suitability as lubricant additives due to their hardness [21].

Researchers have demonstrated a noteworthy impact of NDs when used as ND plate coating in macroscale lubrication. The superior mechanical performance of these ND plates reduced the macroscale COF by fostering an ordered sliding interface [22]. Another study revealed that incorporating annealed NDs in plasma electrolytic oxidation coatings reduced COF and wear volume by 46.67 % and 96.13 %, respectively, compared to plasma electrolytic oxidation coatings. Friction-induced structural transformation of annealed ND particles improved the lubrication and wear resistance [23]. A recent study on lubricants containing ZDDP and NDs solutions via in-situ Quartz Crystal Microbalance (QCM) technique showed the formation of a stiffer reaction films compared to ZDDP only lubricants [24]. Different loading conditions and the presence of NDs showed variations in reaction film formation at different temperatures that impacted the formed film characteristics, however friction performance was not reported [24]. Although some studies have been conducted to comprehend the interactions between NDs and other conventional lubricant additives [19,25], the current understanding of ND compatibility with existing additives remains insufficient.

In the current study, a low friction and low wear lubricant has been developed by incorporating GMO, low concentration ZDDP and NDs with PAO oil. A range of analytical techniques have then been used to explore the fundamental mechanism of tribofilm formation in presence of NDs and its effect on friction and wear at two different temperatures. Particle dispersion stability, size distribution have been obtained by Zetasizer and Transmission Electron Microscope (TEM). The tribofilm properties were analysed by higher resolution transmission electron microscopy (HRTEM). Static secondary ion mass spectrometry (SIMS) was applied to understand the chemical changes on the surface. Improvement in wear performance has been confirmed by the wear volume loss and surface roughness measurement by optical microscope and white light interferometry.

2. Material and methods

2.1. Materials

The organic friction modifier, GMO, along with the primary antiwear additive ZDDP, and the synthetic PAO base oil (Synfluid PAO 6 cSt) were provided by TOTAL Energies, France. Carboxylated NDs in two distinct mediums were purchased from Sigma Aldrich, UK; Detonation Nanodiamonds (DND) with 5 nm diameter dispersed in base oil with 0.1 wt% concentration (type 1) and customised detonated nanodiamonds with same size in dried condition (type 2). Due to limitation of the HRTEM vacuum chamber to characterise the oil dispersed NDs, dried NDs were used to confirm the size and shape of the particles. In accordance with Table 1, nano-lubricants were formulated by diluting dispersed NDs (type 1) to 0.05 wt% in the base oil. The concentration of the additives used here was optimized by varying 0.01 wt%, 0.05 wt%, 0.1 wt%, and 0.3 wt% of NDs with 0.1 wt%, 0.2 wt%, and 1 wt% of ZDDP. Homogeneous dispersion of the particles was achieved by magnetic stirring (500 rpm) for 1 h. Even though the purchasing company was unable to provide the chemical substance used to produce carboxylated NDs due to confidentiality, oleic acid was presumed as a dispersant [26]. In order to confirm the efficacy of the dispersant, the lubricant containing oleic acid was also examined.

Table 1
Lubricant combinations tested.

No.	Lubricant ID	PAO oil wt%	GMO wt %	ZDDP wt %	ND wt %	Oleic Acid wt%
1	PAO	100	0	0	0	0
2	PG	99	1	0	0	0
3	PZ	99.8	0	0.2	0	0
4	PGZ	98.8	1	0.2	0	0
5	PGZOA	97.8	1	0.2	0	1
6	PN0.05 wt%	99.95	0	0	0.05	0
7	PGN0.05 wt %	99	1	0	0.05	0
8	PZN0.05 wt %	99.75	0	0.2	0.05	0
9	PGZN0.05 wt %	98.75	1	0.2	0.05	0

2.2. Nanoparticle and nano-lubricant characterisation

An FEI Titan3 Themis 300 Scanning Transmission Electron Microscopy (STEM) instrument equipped with Gatan Quantum ER energy filter was used to determine the size distribution of ND particles (type 2, in dried condition). The sedimentation experiment was conducted to evaluate the dispersibility and influence of NDs on sedimentation. It was considered one of the most convenient methods to analyse the dispersion stability of nanolubricants [26]. Approximately 10 ml of nanolubricants were transferred from the beaker to the clear tube after preparation. The transparent tubes were positioned in a more observable location for meticulous visual inspection. Eventually, the dispersibility was assessed using a photography method for 1, 15, and 30 days [27,28]. Attenuated Total Reflectance-Fourier Transformed InfraRed spectroscopy (ATR-FTIR) by PerkinElmer, Inc. UK was utilized to observe the surface modification/groups of the carboxylated ND particles [29].

Viscosity of the nanolubricants was measured by Anton Paar Physica MCR301 rotational rheometer, UK. The viscosity of the nanolubricants was similar to the pure PAO 6 base oil even after mixing with different additives due to the low concentration of the additives. Dynamic Light Scattering (Malvern Zetasizer, UK) technique was used to measure the particle size distribution of NDs for two lubricant combinations; PN0.05 wt% and PGZN0.05wt. PN0.05 wt% was chosen as reference lubricant. Because of higher agglomeration, other lubricant combinations were difficult to measure via this process.

2.3. Tribological tests

Tribological tests were carried out using Cameron Plint TE 77 reciprocating tribometer, UK, in accordance with ASTM G 181, similar to an engine condition [30]. The schematic of TE 77 experimental setup is shown in Fig. 1. The cantilever applied the normal load (F_n) on the contacting surface. Frictional force (F_t) was measured with the force transducer, which was used to calculate friction coefficient ($\mu = F_t/F_n$) [31]. Material properties and dimensions of specimens are detailed in Table 2. The sliding tests were performed at 1 GPa contact pressure at two different temperatures 50 °C and 80 °C. Maximum contact pressure was calculated using Hertzian contact theory. The tests were conducted for 2 h at a sliding speed of 0.2 m/s (5.0 mm stroke at 20 Hz). All the experiments were repeated three times to ensure repeatability under a boundary lubrication regime (Lambda ratio, $\lambda < 1$) calculated using Hamrock-Dowson expression [32].

In this study, the test temperatures were selected to simulate real engine conditions in conventional internal combustion vehicles and hybrid vehicles [33]. Before each experiment, plates and pins were cleaned with heptane for 10 min in an ultrasonic bath and air dried. After the experiment, they were cleaned again in heptane to remove

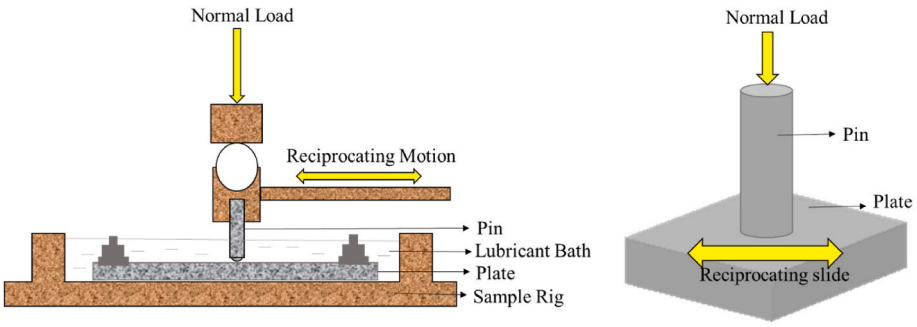

Fig. 1. Schematic of TE 77 experimental set-up. (A colour version of this figure can be viewed online.)

Table 2
TE77 materials properties of the specimen.

Material Properties	Pin	Plate
Material	Steel EN31	Steel EN31
Dimensions (mm)	10 radius	7*7*3
roughness (nm)	401.6 ± 1.2	57.8 ± 1.02
Hardness (HRC)	59.2 ± 0.6	64.8 ± 0.12
Elastic modulus (GPa)	190–210	190–210

remaining oil fragments from the surfaces. Optical white light interferometry (WLI) was used to measure volume loss on pin and plate surfaces after tribological tests. Scanned images of pin surfaces were analysed using Vision64 software from Bruker Corporation. 3D image processing was performed to transform the curve surface into a flat area (to maximum flatness), carefully masking the worn area only. The software curve fitting tool (curvature and tilt) was used to transform the surface so that there was a worn contour in the middle of an undisturbed flat area [34]. Then, the average radius of the wear scar (r), was determined from the worn area. The wear volume loss of the pin was later calculated by using the below equation [31]:

$$V_{\text{pin volume loss}} = \frac{\pi h^2(3R-h)}{3} \quad (1)$$

$$h = R\text{-}((R^2\text{-}r^2))^{0.5} \quad (2)$$

Where,

h = Spherical cap height (μm)
R= Sphere radius (μm)
r = wear scar radius (μm)

The depth of the wear scars on the plate was very shallow, and in some cases, no measurable wear was detected by the white light interferometry. As a result, the roughness of the samples has been measured and reported here. Surface roughness was measured by contact profilometer (Taylor Hobson 120L Talysurf) that uses a 2 μm conical-shaped diamond stylus drawn across the worn surface. Roughness values (R_a) were measured from three different places inside the wear track and averaged for the final R_a value. Later on, pin wear surfaces were analysed by an Optical microscope (Leica Microscope, UK) [31].

2.4. Tribofilm structural analysis

To investigate the tribofilm structure, cross-sections were prepared with High resolution monochromated Focused Ion Beam (FIB, Helois G4 CX Dual Beam). For structural and compositional characterisation, the surfaces were transversely cut using FIB to fabricate cross-sectional lamellar specimens. Then prepared cross-sections were analysed with an FEI Titan3 Themis 300 Scanning Transmission Electron Microscopy (STEM) instrument equipped with Gatan Quantum ER energy filter, Energy Dispersive X-ray (EDX) and High-Angle Annular Dark-Field Scanning (HAADF).

With a high-performance cold field emission (CFE) SEM (Hitachi SU8230), the wear tracks on the plate surfaces were analysed before and after EDTA solution was applied to remove the tribofilm on the wear track to understand the surface wear mechanism [35]. The measurements were carried out at a beam voltage of 2.0 kV and images were acquired at different magnifications.

A Dimension Icon Bruker AFM, USA, in Peak Force QNM mode was employed to image the surface morphology and adhesion profile of the wear surfaces. A silicon probe and a 125 μm long cantilever, comprising a lever force constant of 40 N/m and resonant frequency of about 300 kHz were used. The AFM images were obtained with a scan rate of 1 Hz across various selected areas with dimensions of 100 nm × 100 nm, 500 nm × 500 nm, 1 μm × 1 μm and 5 μm × 5 μm followed by the phase analysis using the tapping mode.

Static SIMS measurements were performed on the steel plates after the tribological tests °using a Hiden Compact SIMS, equipped with a MAXIM-600P detector. The detector has a Hiden 6 mm triple quadrupole mass filter and features pulse ion detection capabilities. The static SIMS uses the following conditions: Ar^+ primary ion with ion energy 5000V, emission 10.0 mA. The measured mass (m/Z) range was between1-300. The sample area for positive and negative spectra is 800 x 800 μm^2. All the measurements were taken inside and outside of the wear track at two different locations to ensure reproducibility.

3. Result and discussion

3.1. Nanoparticle and nanolubricant characterisation

Fig. 2(*a*) shows the HRTEM image of customised driedcarboxylated ND particles, whereas (*b*) shows their size distribution. Fig. 2 (*b*) demonstrates that the range of ND size varied between 6 and 18 nm, which is very close to the range of 5 nm mentioned by the supplier. The variation in size is caused by the agglomeration of the ND particles due to their surface attraction forces [36]. Fig. 2 (*c*) illustrates FTIR spectra for the carboxylated ND particles. Here, the absorption bands of C═O bond stretching at 1113 cm^{-1}, hydroxyl bond –OH bending at 1629 cm^{-1}, carbonyl bond C═O stretching at 1773 cm^{-1}, and hydroxyl bond –OH stretching at 3424 cm^{-1} are visible from the spectra. These absorption peaks are characteristic peaks for the carboxylated ND peaks found in other literatures as well. Hence, from the FTIR analysis, functional group of the NDs were confirmed to be carboxylated modified [29,37].

Fig. 3 shows the sedimentation observations indicating the dispersibility of NDs in PAO oil, PAO with GMO, PAO with ZDDP, and PAO, GMO and ZDDP combinations. No changes are observed upon visual inspection after 30 days. In addition, no solid–liquid separation is observed for any of the PAO oil, additives and ND combination, even after 30 days of observation.

The stable dispersibility has resulted from the functional groups adsorbed on the surface of NDs because of the chemical modification by the provider company [26]. The photographic observation showed that adding a small concentration of additives and NDs did not impact

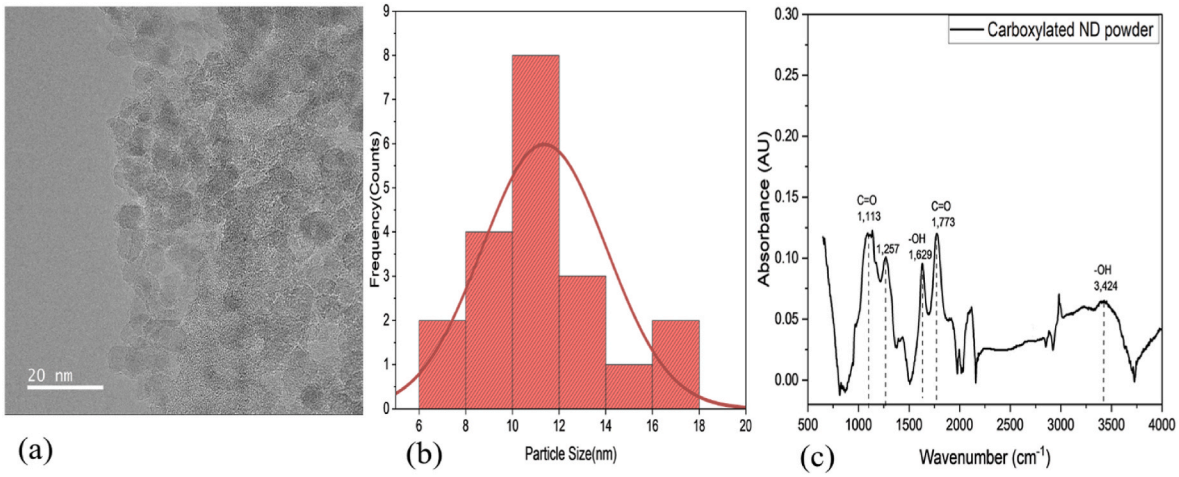

Fig. 2. (a) HRTEM image of NDs, (b) Particle size distribution of NDs in dry environment, (c) FTIR analysis of carboxylated ND powder. (A colour version of this figure can be viewed online.)

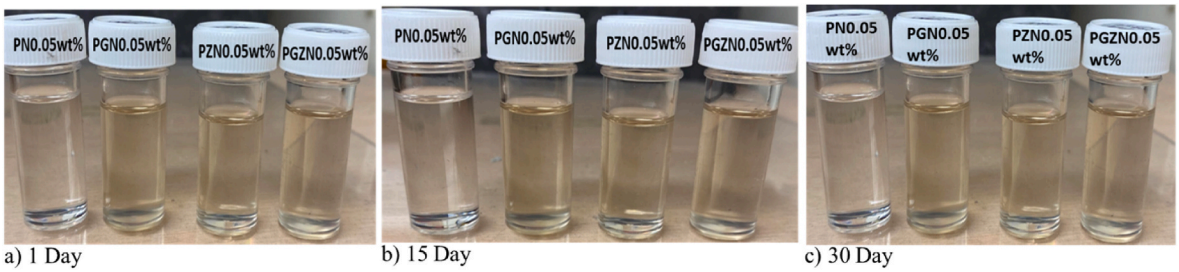

Fig. 3. Visual observation of NDs sedimentation in lubricant combinations for a) 1 day, 2)15 days, c) 30 days. (A colour version of this figure can be viewed online.)

sedimentation behaviour. Due to the low concentration of NDs, it became difficult to differentiate whether there is any sedimentation in the lubrication combination by visual inspection. As the NDs were commercially dispersed, certain surface modifications were involved to make them dispersed in oil medium by the supplying company. However, due to confidentiality, the supplier could not disclose the process or chemicals used for surface modification of NDs. As the NDs were carboxylated and from previous research, it was found that carboxylic nanoparticles are oleophilic, so they can be well dispersed in an oil medium. Hence, the mechanism for the dispersibility of NDs is caused by the carboxylate surface functionality [38]. From the photographic observation, no sedimentation is found even after 30 days. However, with DLS measurement, agglomeration of ND particles is observed after 30 days. The agglomeration might have happened due to the surface interactions between nanoparticles [36].

Further, Malvern Zetasizer was employed to measure the particle size distribution of NDs in liquid medium. At room temperature, lubricant combinations of PN0.05 wt% and PGZN0.05 wt% were used for the particle size distribution measurement. Fig. 4 shows the nanoparticle size distribution curves of PN0.05 wt% and PGZN0.05 wt% nanolubricants with different additive combinations.

Due to the higher concentration of the received nanolubricant, it could not be used in this measurement because it requires dilution. Hence, the lubricant combination PN0.05 wt% was selected as the reference for this measurement to maintain the accuracy of the experiment. Fig. 4(a) shows the average particle size of NDs in lubricant combination ranging from 30 to 31 nm immediately after formulation. The size of the nanoparticle tends to be different from the size measured from the HRTEM image and nominal size (~5 nm) provided by the company for both scenarios, the measurements were done for dried

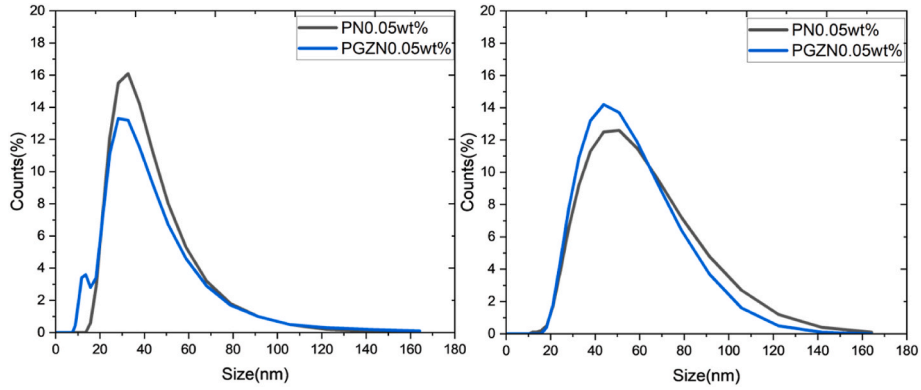

Fig. 4. NDs particle size distribution for PN0.05 wt% and PGZN0.05 wt% lubricant combinations after (a) immediate preparation and (b) 30 days later. (A colour version of this figure can be viewed online.)

nanoparticles (not dispersed in base oil). Fig. 4(b) shows that after 30 days of nanolubricant preparation, the size varied from approximately 43-50 nm. Hence, when nanoparticles were mixed with base oil, agglomeration happened due to attractive interactions between nanoparticles resulting in an increase in size that was visible from the DLS measurement [36,39]. Further analysis is required to stabilise the nanolubricant combination for more extended storage capability. To avoid any effect of particle agglomeration on tribological performance, all tribology experiments were done immediately after preparing the nanolubricants.

3.2. Frictional performance analysis

The graph in Fig. 5 illustrates the evolution of the friction coefficient (COF) over time for various lubricant combinations, both with and without NDs, at two different temperatures. The results showed apparent differences in the frictional coefficient for different lubricant combinations without ND at 50 °C and 80 °C (Fig. 5a and *b*). PAO oil exhibited the highest coefficient of friction for two different temperatures than any other combination. PG blend displayed lower COF than PAO oil at both temperatures, which is expected as GMO has a linear molecular structure and adsorption of GMO occurs at low temperature on an iron surface, known as physisorption. This phenomenon contributes to friction reduction within the low-temperature range. However, physisorption is reversible and related to temperature. With the increase in temperature, the COF for PG increased gradually, which might have been caused due to desorption at higher temperatures (80 °C) [40]. For the PZ combination, the COF increased with increasing temperature, and the COF is higher than PG, as reported in the literature [41]. One of the reasons could be that at a higher temperature, lubricants with ZDDP

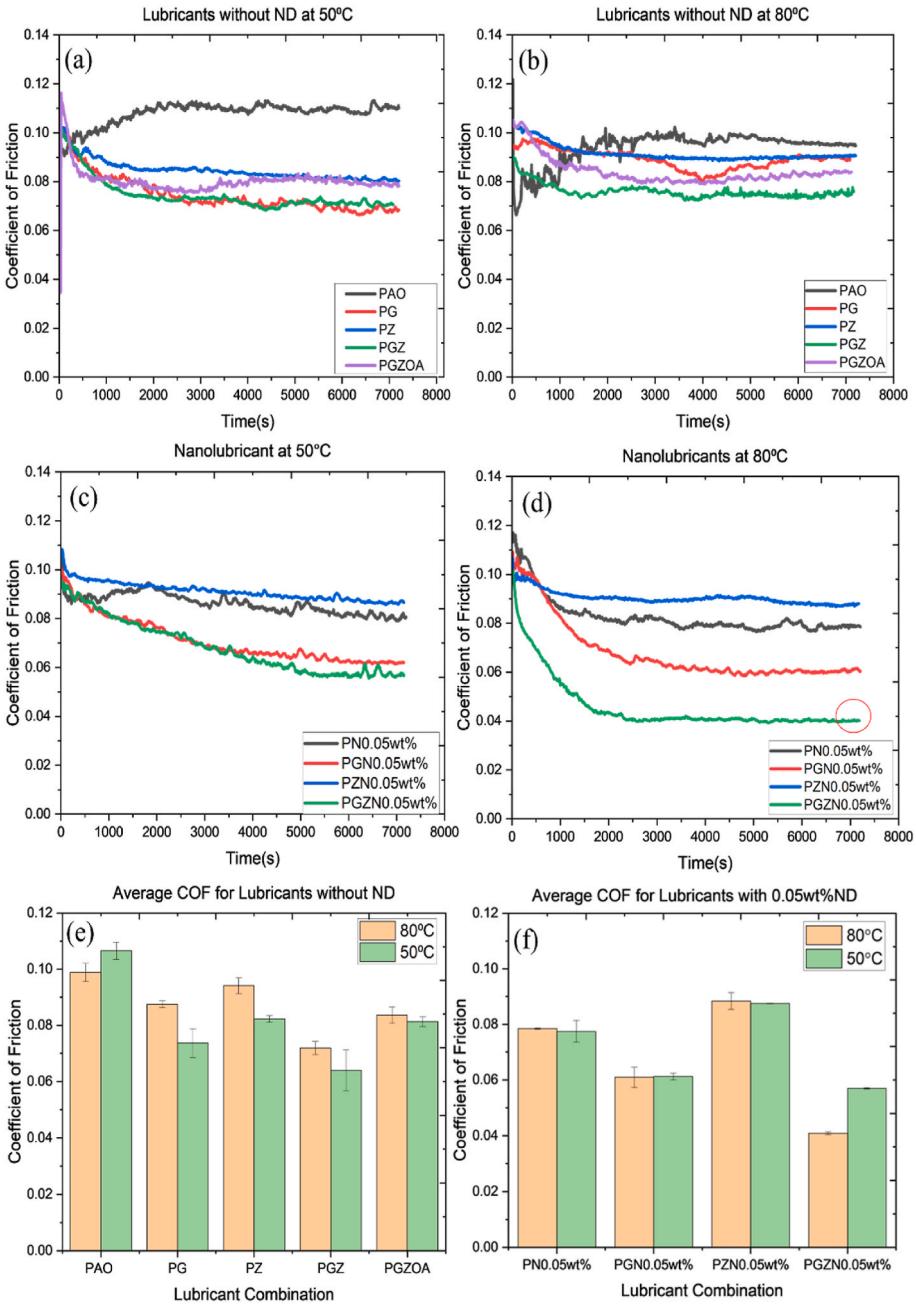

Fig. 5. Effect of NDs on COF for different lubricant combinations at (a) 50 °C, (b) 80 °C, Effect on COF without NDs for different lubricant combinations at (c) 50 °C, (d) 80 °C, Average COF for last 30 min of tribotests for (e) Lubricant combination with 0.05 wt% of NDs at 50 °C and 80 °C, (f) Lubricant combination without NDs at 50 °C and 80 °C. (A colour version of this figure can be viewed online.)

develop higher phosphate chain lengths on the top layer of the tribofilm [42]. These films have a thick pad-like structure that inhibits fluid entrainment on the contacting surface [43,44]. Elevated temperatures led to a rise in friction. The difference in COF for the PGZ lubricant combination for both temperatures is not significant, as the temperature difference window is narrow. However, the synergistic effect between GMO and ZDDP resulted in lower COF (~0.08) than PAO oil due to the preferential adsorption of GMO on steel surface [45]. The addition of Oleic acid to the lubricant combination did not considerably impact COF reduction. This suggests that the reduction in friction is not primarily due to the addition of Oleic acid, utilized as a dispersant in nano-lubricant formulation.

Fig. 5(c) shows variation in COF for nanolubricant containing 0.05 wt% of NDs at 50 °C. It showed that at the lower temperature, the COF reduced to approximately 0.08 for PN0.05 wt%, which is much lower than the PAO oil. For PGN0.05 wt% lubricant combination, COF became approximately 0.07 whereas for PZN0.05 wt% lubricant, the friction did not reduce; instead, it is almost the same as the lubricant PZ without NDs. Nevertheless, for the lubricant combination PGZN0.05 wt%, the COF was approximately 0.06 which is lowest in comparison with other lubricant combinations at 50 °C. Fig. 5(d) shows variation in COF for nanolubricant containing 0.05 wt% of NDs at 80 °C. All four lubricant combinations exhibited greater stability in COF compared to that at 50 °C where PGZN0.05 wt% showed the lowest frictional coefficient. In addition, the running in time is also shorter at 80 °C.

Fig. 5 (e) and *(f)* show the average coefficient of friction for lubricants without NDs and with 0.05 wt% NDs at 50 °C and 80 °C. The average COF is calculated by averaging the last 30 min of frictional coefficient values which is in the stable phase. It is found that the COF did not change much with temperature differences. Again, ZDDP is an anti-wear additive and temperature has significant impact on the formation of ZDDP tribofilm [40,41]. Development of ZDDP tribofilm will increase friction and reduce wear due to the formation of glass like phosphate tribofilm. In this study, COF for PZN0.05 wt% is higher than the PN0.05 wt% for both the temperature, which can be attributed to the formation of ZDDP tribofilm. The slight improvement in COF is due to the polishing effect of NDs present in the PN0.05 wt% lubricant combination [46].

However, a substantial reduction in COF from 0.06 to 0.04 could be observed for PGZN0.05 wt% lubricant combination at elevated temperature. The frictional curve in Fig. 5(d) showed a more stable state after 40 min of sliding. The reduced frictional coefficient is due to the synergistic effect of the PGZN0.05 wt% lubricant combination. From Fig. 5, it can be concluded that the lowest COF is obtained for PGZN0.05 wt% lubricant combination at 80 °C. Improvement in frictional properties is visible when compared without NDs. The addition of NDs in the lubricants significantly reduced COF, which is not observed in any other pure or nanolubricant combination.

3.3. Wear surface analysis

After 2 h of sliding tests, the wear surface of the pins was analysed by optical white light interferometry (WLI) to understand the anti-wear characteristics of different lubricant combinations. Fig. 6 shows the average wear volume of pins after sliding in lubricants (*a*) without NDs and (*b*) with NDs. The wear volume of the pin tested in base oil increased with temperature (Fig. 6(a)). Because of the low viscosity, asperity contact increases with harsher lubrication conditions resulting in increased wear for PAO oil [42]. For PG lubricant, the wear volume loss did not change considerably as it didn't show any anti-wear properties with steel surfaces. However, the wear volume loss of the pin for PZ sample is lower than the other combinations at same temperature. The effectiveness of ZDDP as an excellent anti-wear additive was the driving factor for this outcome. It prevents metal to metal contact by forming thick solid pad like tribofilm on the rubbing surfaces [47]. Even though it results in higher friction, this pad like structure effectively lessens wear by producing protective phosphate glass based tribofilm [4]. An increase in phosphate chain length is observed on the wear scar with increasing the temperature that resulted in lower wear [44,48,49]. The higher phosphate chain length of the tribofilm is related to lower wear rate at elevated temperature [50]. Hence, the anti-wear property of ZDDP tribofilm is the reason for PZ lubricant to cause lower wear volume loss of the pin. In contrast, the other combinations have a little impact on wear performance at the same temperature.

Fig. 6(b) shows that the addition of NDs with the additive combinations reduced the wear of the pin at 80 °C, which is not the case for 50 °C. An antagonistic effect for the PN0.05 wt% lubricant combination is found at 50 °C that could delay formation of thermal reaction film and generate more abrasive particles that ultimately increased the wear [47,51]. For the PZN0.05 wt% lubricant, it is noteworthy that the wear volume loss of the pin is lower than other combinations. The observed result can be ascribed to the generation of a glass phosphate tribofilm by ZDDP on the contacting surfaces, which functions as a protective barrier at both temperatures [52,53]. Again, inclusion of NDs which are known to have higher hardness, exhibits polishing effect on the contacting surfaces further contributing to protect the contacting area [46,54]. Prior studies have demonstrated the existence of a synergistic response resulting from the combination of NDs and ZDDP. Incorporation of NDs in ZDDP formulation increased film thickness which facilitated better adhesion to the substrate [46]. Our experimental findings align with these previous outcomes, revealing the existence of a substantial synergistic effect that significantly reduced wear for PZN0.05 wt% lubricant combination at both temperatures.

From the manufacturer and HRTEM analysis, it is verified that the NDs are spherical in shape, which potentially assisted to change the sliding friction to rolling friction, leading to a reduced COF in the lubricating system [55]. Researchers have shown that the hardness of NDs reduced the sharpness of the asperity contacts, resulting in

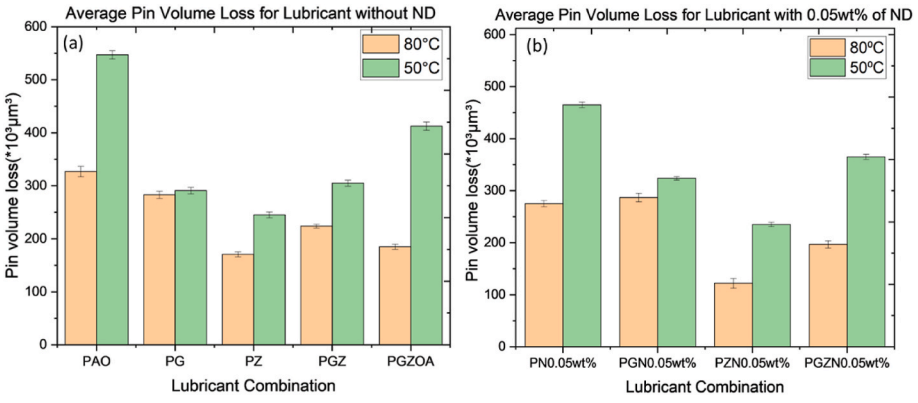

Fig. 6. Average wear volume loss of pin surfaces. (A colour version of this figure can be viewed online.)

polishing effect and further reduced friction and wear [54]. Fig. 7 shows the optical microscopic images of pin surfaces tested under NDs lubrication at 80 °C. Differences in the degree of wear found to be apparent for different lubricants. The lowest width (average) was attained for PZN0.05 wt% pin surface. The polishing effect is visible for PGZN0.05 wt% lubricated pin surface. Even though PGN0.05 wt% also showed a polishing effect, it is not as significant as PGZN0.05 wt%. *Fig. 6(b)* illustrates that the addition of NDs in the lubricating system improved the wear compared to the individual lubricating system without NDs. This improvement is further established from plate wear scar analysis by SEM in Fig. 8. This can be credited to the smoothening effect of NDs with different additives in the lubricant combination. It is worth noting that the addition of NDs did not consistently reduce wear at 50 °C temperature. At 80 °C temperature, lubricants with NDs did not substantially reduce wear but had no adverse effect on wear properties.

3.4. Wear mechanism

The SEM images from Fig. 8 depicts the changes in surface morphology on the plate wear track. Deep groves were observed for pretest plate (*a*), whereas base oil tested plate (*b*) and PN0.05 wt% lubricated plate(*c*) demonstrated abrasive wear.

From morphological observation by SEM shown in Fig. 8, PGN0.05 wt% (*d*) and PZN0.05 wt% (*e*) lubricated plate surfaces showed lower abrasion than PN0.05 wt% lubricated surface. PGZN0.05 wt% (*f*) lubricated plate surface displayed a much smoother surface than other plates. The abrasive grooves are higher for base oil and PN0.05 wt% lubricated surfaces, whereas for PGN0.05 wt% and PZN0.05 wt%, fine grooves are visible that evidenced the presence of rolling effect due to NDs [56]. The bar graph in Fig. 9 illustrates the average surface roughness of plate wear surfaces. It is clear from the SEM images and surface roughness measurement that the lubricant combination PGZN0.05 wt% reduced the surface roughness significantly compared to others. The lubricant combination PGN0.05 wt%, PZN0.05 wt% and PGZN0.05 wt% reduced the average roughness of the plate surfaces and the possible mechanism is polishing effect of the NDs [57]. The hardness of the NDs reduced the sharpness of the asperity contact, resulting in polishing effect [54]. From the current results and discussion, it can be ascertained that the inclusion of NDs in the lubricating oil combination improved the tribological properties of lubricating oils compared with lubricants without NDs.

Based on the above frictional and wear characteristics, it is evident that at 80 °C, the lubricants with and without NDs performed better than at 50 °C temperature. Also, evidence of synergistic effect is visible for the PGZN0.05 wt% lubricant combination that needs further analysis to understand the possible mechanism of reduced friction and wear performance. The following sections present the results from advanced analysis of tribofilms formed from PGZ and PGZN0.05 wt% lubricant combinations at 80 °C.

3.5. Tribofilm formation and characterisation

HRTEM was used to analyse the details of the tribofilms formed on the steel surfaces for two different lubricant combinations, PGZ and PGZN0.05 wt% at 80 °C as shown in Fig. 10. The upper layer is the Pt layer for the FIB cross-section, middle layer is the formed tribofilm and the lower part is the steel substrate. A noticeable disparity in tribofilm thickness is identified in the cross-sectional view of the tribofilms for both lubricant combinations. Fig. 10(*a*) shows that a thin tribofilm (average thickness 3–5 nm) is formed after 2hrs of sliding in PGZ lubricant. The incorporation of 0.05 wt% NDs in the lubricant combination indeed increased the tribofilm thickness to an average of 20–22 nm. This study is the first to experimentally demonstrate the formation of a thick homogeneous tribofilm developed from the PGZN0.05 wt% nanolubricant where NDs structures are evidently visible. Thus, the addition of NDs had a synergistic effect on tribofilm formation that reduced the friction, which is not identified for other lubricant combinations.

Fig. 11 (*a*) and (*b*) exhibit the cross-section of the tribofilm for the lubricant combination PGZN0.05 wt% where the presence of NDs inside the tribofilm is clearly visible. From Fig. 11 (*c*) and (*d*), it is found that NDs adhered in a scattered manner inside the tribofilm layer. The magnified HAADF image of the tribofilm cross-section in Fig. 11 (*e*) verified the notion further and proved the presence of spherical ND elements of variable sizes trapped inside the formed tribofilm. The lattice spacing between the ND layers is 0.206 nm shown by the arrow in Fig. 11(*b*), which agrees with the literature [58].

EDX was used to further analyse the chemical nature of spherical elements in the tribofilm illustrated in Fig. 12. The tribofilm consists of Zn, P, S and O enriched layers and the black spherical shaped elements are identified as NDs in the form of carbon elements. NDs might have slightly agglomerated in the lubricant combination due to their affinity towards nearby nanoparticles [39]. Hence, one possibility could be that these NDs later on, due to high shear stress broke down into smaller sizes

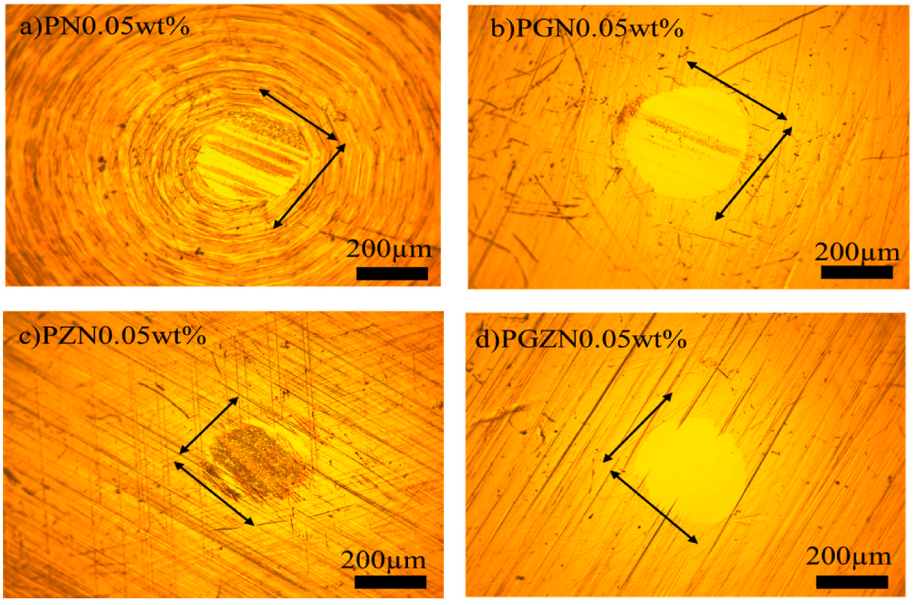

Fig. 7. Optical Microscope images for pin wear surfaces of lubricants with NDs at 80 °C. (A colour version of this figure can be viewed online.)

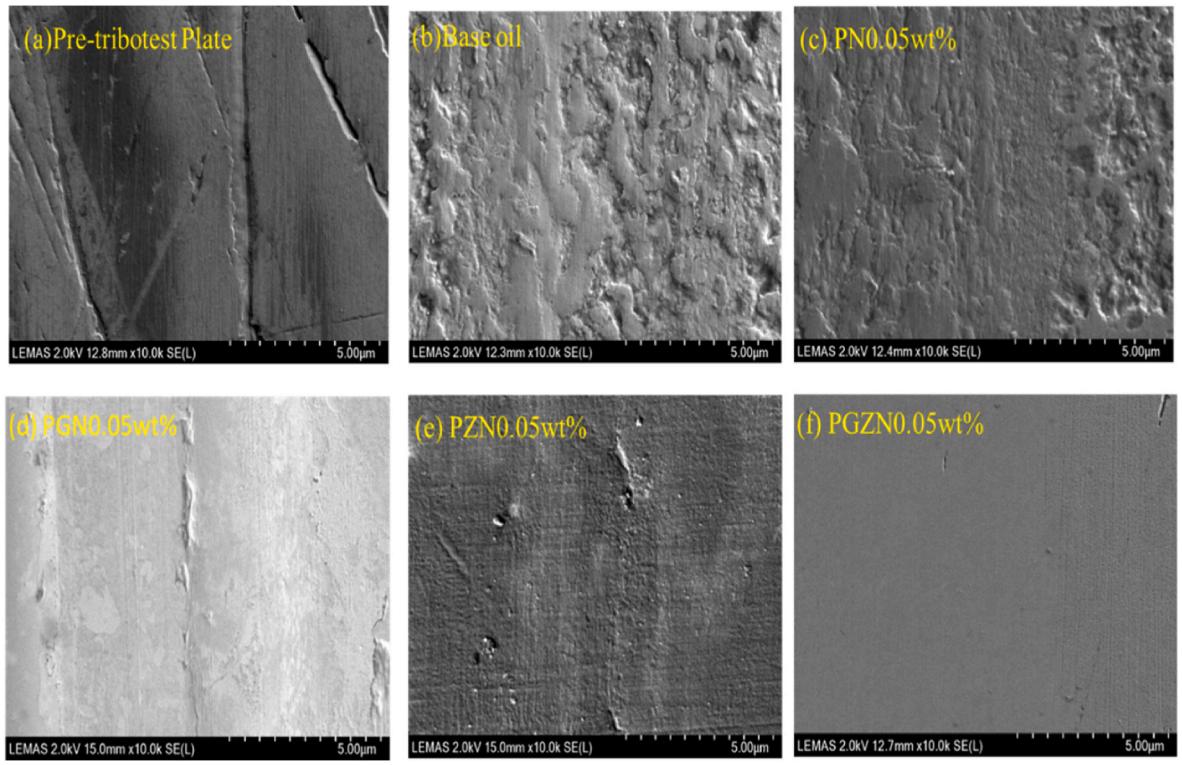

Fig. 8. Surface analysis of the wear scars on plate samples following tests with lubricant combinations at 80 °C by SEM. (A colour version of this figure can be viewed online.)

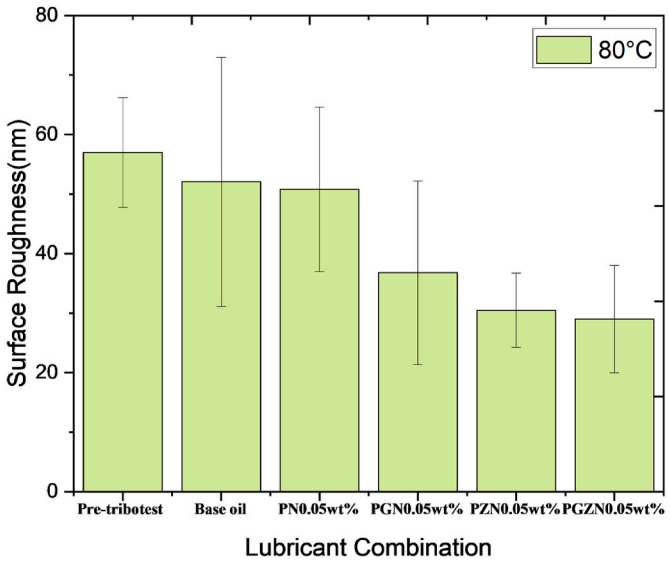

Fig. 9. Surface roughness measurement of plate wear scar for lubricant combinations with NDs after 2hr tribological tests. (A colour version of this figure can be viewed online.)

and rolled inside the tribofilm [21,54,56]. Fig. 12 shows NDs are embedded on the tribofilm uniformly and, with EDX analysis the homogeneous distribution of NDs inside the tribofilm is confirmed.

Fig. 13 validated that the tribofilm is enriched with NDs and distributed uniformly. Line EDX scanning of the tribofilm section and atomic fraction of the elements from the table indicated an abundance of C elements in the wear track even though the concentration of NDs in the lubricant combination is minimal, about 0.05 wt%. Hence, the presence of NDs in the lubricant combination has a synergistic effect that increases the tribofilm thickness, resulting in lower COF and wear.

3.6. Change in surface adhesion and analysis of phase profile

The wear surfaces of the PGZ and PGZN0.05 wt% lubricant combinations at 80 °C were analysed using Atomic force microscope. Fig. 14 shows the 2D and 3D profiles of height, adhesion of the wear tracks. The topography and adhesion were measured by PeakForce QNM mode. Fig. 14 (*a*), (*c*), (*d*) and (*f*) revealed apparent differences in topographical characteristics for the lubricant combinations. PGZ tribofilm, shows a tribofilm with a pad-like structure as expected [59]. The supplementary data in Figure A3 shows the prominent pad like structure of ZDDP tribofilm on the PZ and PGZ lubricated steel surfaces, tested at 80 °C. In contrast, no pad like structure or channels are visible on the PGZN0.05 wt% tribofilm (Fig. 14(d)). The presence of spherical NDs is noticeable from the 3D profile of Fig. 14 (*f*) of PGZN0.05 wt% tribofilm. Furthermore, the adhesion map obtained from the PGZN0.05 wt% tribofilm (Fig. 14 (*e*)) shows lower adhesion areas to correlate with the positions of spherical NDs.

Oblak and Kalin explored the adhesion properties and macroscopic friction for tribofilms developed on the steel and DLC coatings [60]. Their study suggests that macroscopic friction is directly correlated with adhesion properties. Tomale et al. reported that the development of ZDDP tribofilm amplifies the adhesion force [61]. Kaisei et al. also reported that the friction may increase because of the higher adhesion property of ZDDP [62]. These analyses also support the results in the current study; COF increased with ZDDP addition. According to the literature, the diameter of the nanoparticles and the nature of the tail group of nanoparticles thin coating highly modulates the adhesion force [60]. The adhesive force of the functional groups depends on factors such as electrostatic forces, capillary forces, van der Waals force, dipole-induced force, and H–bonding. Hydrophilic nanoparticles have high polarizability which develops attractive forces such as H-bonding, as well as capillary forces and electrostatic forces, towards the silicon probe contributing to the higher adhesive force. On the other hand, hydrophobic or lipophilic carboxylated nanoparticles increase the

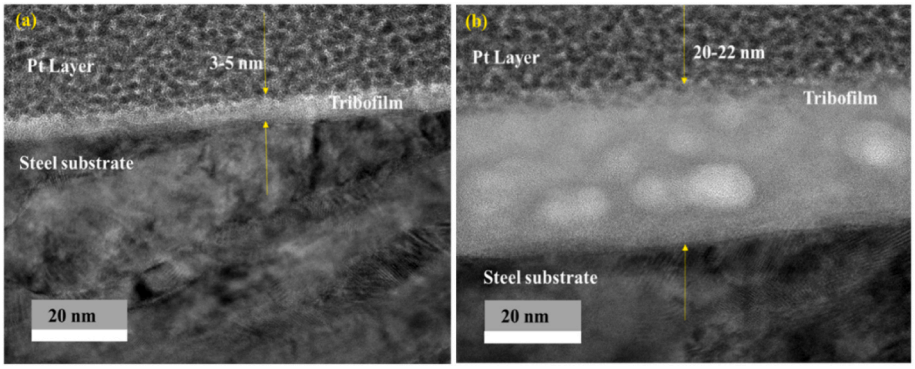

Fig. 10. HRTEM images for formed tribofilm at 80 °C for (a) PGZ and (b) PGZN0.05 wt%. (A colour version of this figure can be viewed online.)

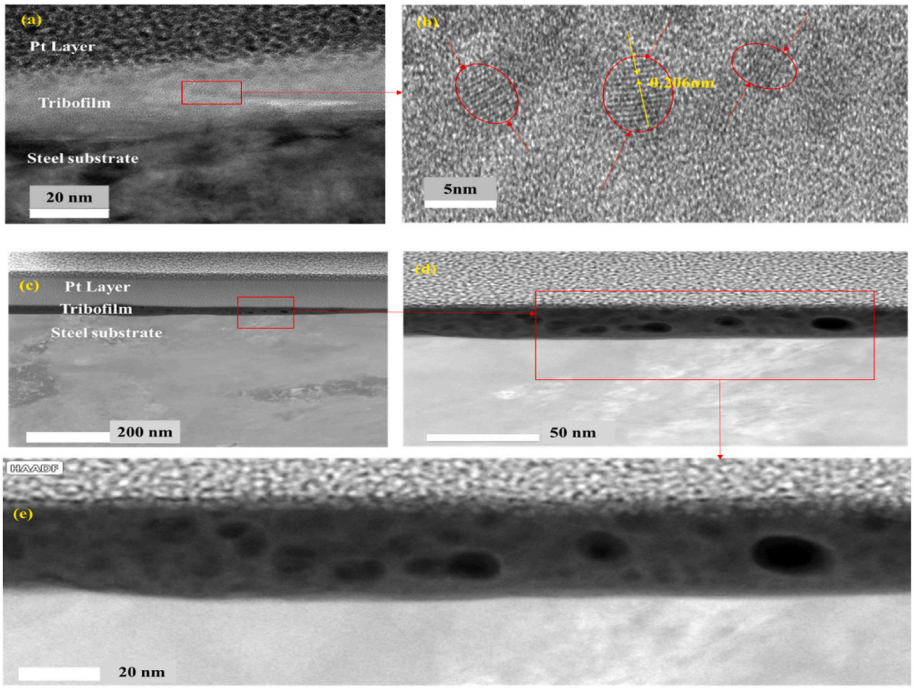

Fig. 11. HRTEM image of PGZN0.05 wt% tribofilm after 2 h of tribotest. (a) Cross sectional view of tribofilm layer,(b) NDs found to be embedded on the tribofilm, (c) HAADF image of the tribofilm, (d) Magnified image of the indicating area, (e) HAADF image showing clear presence of NDs embedment. (A colour version of this figure can be viewed online.)

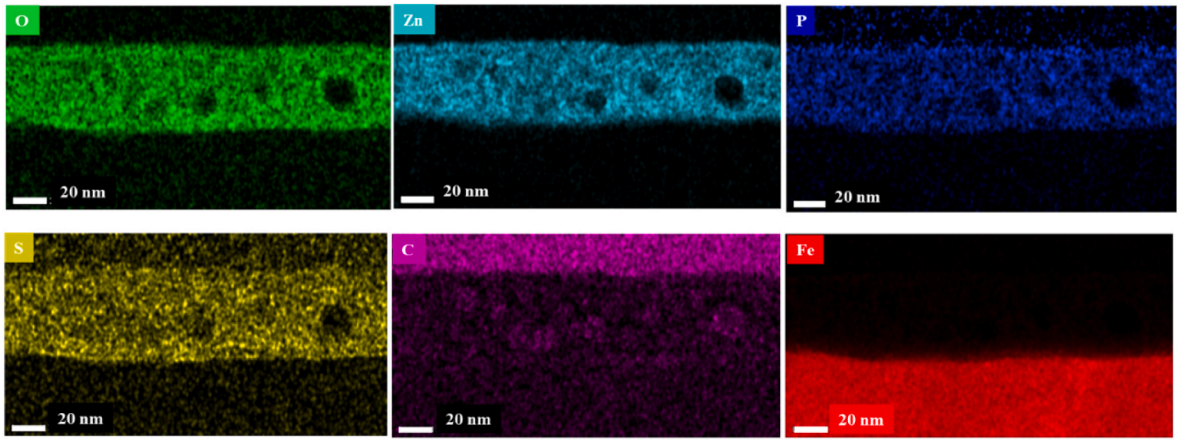

Fig. 12. EDX measurement by HRTEM for PGZN0.05 wt% tribofilm cross section showing NDs from an area indicating O, Zn, P, S, C and Fe elements. (A colour version of this figure can be viewed online.)

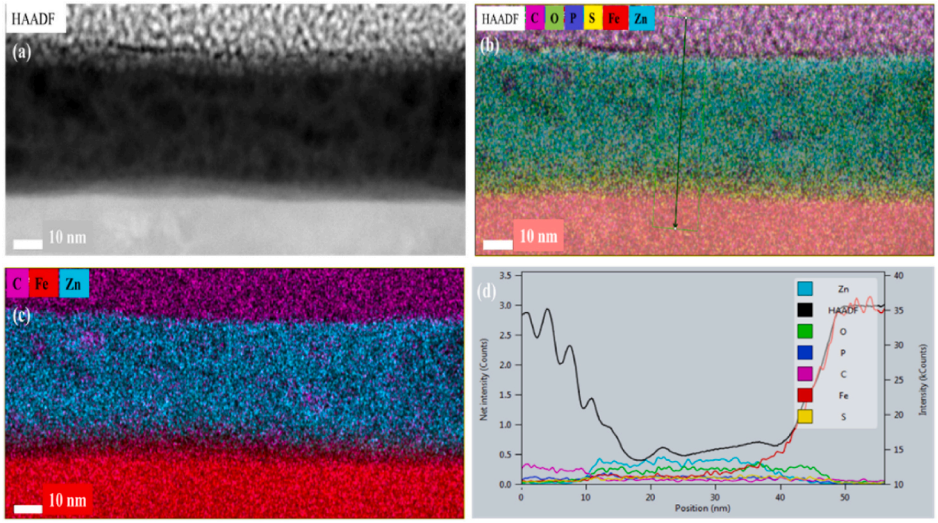

Element	Atomic Fraction (%)
CK	24.44
OK	21.51
PK	3.44
SK	3.32
CrK	0.59
FeK	38.95
ZnK	7.76

Fig. 13. HAADF image of (a) PGZN0.05 wt% tribofilm cross-section, (b) EDX line measurement of the cross-section, (c) EDX measurement for area showing C, Fe, Zn elements, (d) elemental intensity from line measurement and Table showing atomic fraction for different elements present in the tribofilm. (A colour version of this figure can be viewed online.)

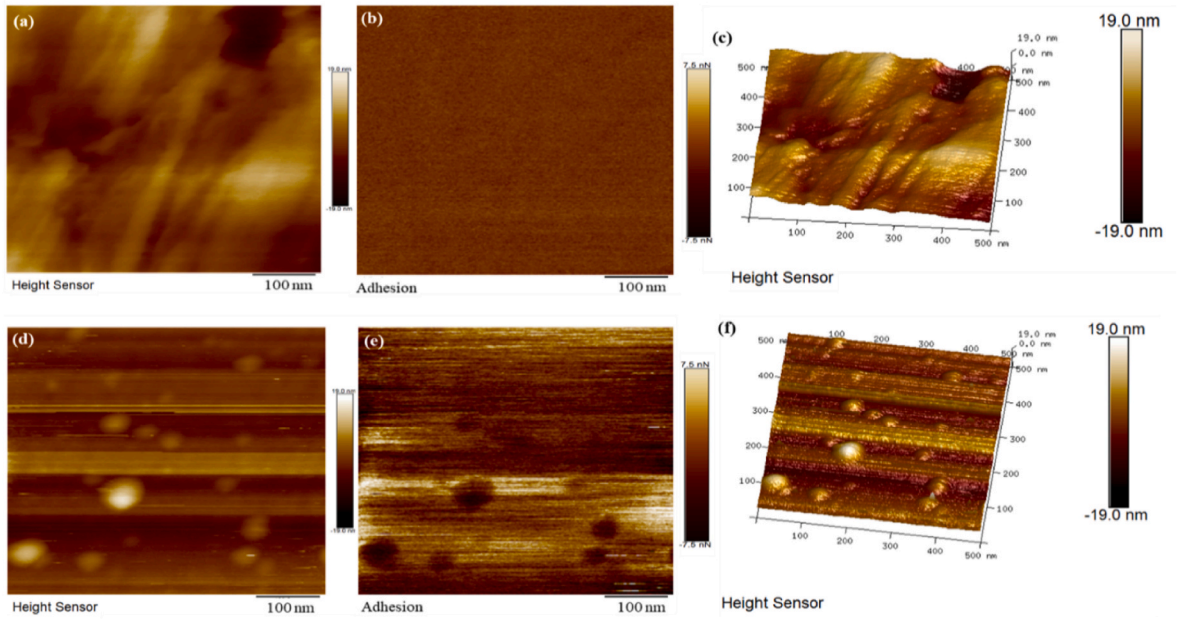

Fig. 14. Surface topography analysis by AFM for PGZ tribofilm (a) 2D height profile, (b) Adhesion profile, (c) 3D height profile and for PGZN0.05 wt% tribofilm (d) 2D height profile, (e) Adhesion profile, (f) 3D height profile. (A colour version of this figure can be viewed online.)

reactivity with airborne contaminants which prevents H-bonding or capillary forces by hindering the water meniscus formation with the cantilever tip [63]. This is in line with the current data set, which shows influence of adhesion response based on the functionalization and size of the nanoparticles. Fig. 14(*e*), the adhesion profile indicates the spherical darker regions have negative adhesion because of the functional group of the nanoparticles than the adhesion value for the lubricant with organic friction modifier and ZDDP in Fig. 14(*b*).

For phase analysis, a Tapping mode atomic force microscope (TM-AFM) was used. Principally, the phase images were produced depending on the phase lag between oscillation frequency of the driver and cantilever where phase lag reflected the interface between sample surface and cantilever tip. Therefore, phase shifts or phase lags are results of the attractive and repulsive forces developed due to the interactions between the AFM tip and the sample surface. Attractive forces result in negative phase shift and positive phase shift occurs when repulsive force acts between the cantilever tip and relatively stiff surfaces [64,65].

Different studies have also shown that chemical characteristics like hydrophobicity has an impact on surfaces that affect the phase shift [38, 66]. From research, it has been determined that carboxylated nanoparticles are lipophilic in nature and lipophilic or oleophilic substances are considered as hydrophobic as well [38]. Researchers have addressed that surfaces of higher elastic modulus result in brighter or larger positive shift due to their hydrophobic or lipophilic nature [67]. Fig. 15 show PGZ tribofilm, (*a*) height profile, (*b*) phase shift, and for PGZN0.05 wt% tribofilm (*c*) height profile, (*d*) phase shift obtained after 2hrs of tribological tests. The phase image is in agreement with the 3d height profile (*c*) of Fig. 14. It showed the characteristic pad like structure of ZDDP tribofilm. The phase shift is in the negative range for PGZ tribofilm. Nevertheless, for the PGZN0.05 wt% tribofilm, the phase shift has

shown different features that were also addressed by B. Acharya et al. [24]. He suggests that the phase profile confirmed the embedment of nanoparticles inside the tribofilm, similar to current findings. The phase profile for PGZN0.05 wt% tribofilm shows brighter contrast than the PGZ tribofilm, indicating the presence of NDs on the tribofilm [24]. Dong and Yu et al. also mentioned that the brighter contrast or positive phase shift occurs due to more substantial elastic properties with larger Young's modulus of the nanoparticles [64]. With the phase profile shown in Fig. 15(*d*), it can be suggested that the addition of NDs in the lubricant combination of PGZN0.05 wt% could also increase the stiffness of the tribofilm resulting in positive phase shift. Moreover, the change in phase shift is due to the presence of lipophilic NDs on the surface.

Surface topography and characteristics were further confirmed by SEM analysis. Fig. 16 shows the surface morphology of (*a*) PGZ tribofilm and (*b*) PGZN0.05 wt% tribofilm. Both images are in complete agreement with the features explained for the AFM images of the tribofilms. The PGZ tribofilm has pad like structure and the PGZN0.05 wt% tribofilm has NDs of spherical shape embedded on the wear track. The presence of the NDs of different sizes has been confirmed by the magnified images of the wear track of unetched PGZN0.05 wt% surface (Fig. 16 (b)). SEM images shows that small spherical nanoparticles are present on the wear track. It proves that NDs embedded on the wear track might have the polishing effect to make the surface smooth [16,55,68]. NDs used in PAO oil or with ZDDP, played an effective role to reduce friction and wear by rolling and polishing mechanism [5,24]. In our lubricant combination, NDs with a low concentration of 0.05 wt% with GMO and ZDDP was used. GMO itself is an organic friction modifier and with the current lubricant combination, it certainly reduced friction due to synergistic effect [14]. The friction and wear measurement confirmed that the coefficient of friction has been reduced for PGZ and PGZN0.05 wt% lubricant combinations. However, other lubricant combinations did not reduce the coefficient of friction; instead, they worked as single additive systems.

3.7. Tribofilm chemical characterisation

Fig. 17 shows the Static SIMS analysis for the PGZ and PGZN0.05 wt % lubricant combination at 50 °C and 80 °C. Here, (*a*) and (*b*) shows the difference in positive ion spectra, and (*c*), (*d*) show the difference in negative ion spectra for PGZ lubricant at two different temperatures. From the ion spectra, the ion fragments associated with ZDDP decomposition can be observed at both temperatures. Nevertheless, for both positive and negative ion spectra at 50 °C, the intensity of ZDDP decomposition ions is very low. Whereas for ion spectra at 80 °C, the ZDDP decomposition ions are more pronounced in intensity for both positive and negative ion spectra. Even though at both temperatures, the ZDDP corresponding phosphate ions ($[PO_2]^-$ and $[PO_3]^-$) were not detected but other metaphosphate elements like $ZnP_2O_6^-$, $ZnP_2O_7^-$, $ZnP_3O_6^-$ are successfully detected in the tribofilm formed at 80 °C. Iron hydroxides, iron oxide and sulphide elements were also not found that are usually seen for ZDDP decomposed species [41]. Detailed analysis can be found in supplementary data. The reason for not successfully detecting sulphate/sulphide species, phosphates, thiophosphates, is that in usual lubricant combinations higher concentration of ZDDP (1.2 wt% or 3 wt%) has been used but in this work low concentration of about 0.2 wt% ZDDP has been used [48,69]. Even with this low concentration, ZDDP tribofilm is formed although ZDDP decomposed elements were not prominently visible in Static SIMS analysis. It proved that ZDDP film is formed however, GMO influenced ZDDP decomposition and restricted the adsorption of ZDDP on the surface which varied with varying temperatures [14]. In previous works, it has been proposed that GMO hydrolyses and forms oleic acid which is then adsorbed on the steel surfaces preventing metal to metal contact [70,71]. Moreover, when GMO is used with ZDDP a competitive adsorption phenomenon occurs between the additives and as GMO has higher affinity towards the steel surfaces due to the presence of polar head group, it hinders the adsorption of ZDDP decomposed products on the surface. These further creates a synergistic effect between GMO and ZDDP that improves frictional properties of the tribological system at higher temperature [14,72]. Researchers have shown that the rate of chemisorbed ZDDP film formation is highly influenced by temperature and above 80 °C the chemisorbed ZDDP is formed but at lower temperature the film formation rate is not substantial [73]. Hence at 50 °C temperature, as the ZDDP film was not fully formed therefore the competitive adsorption phenomena did not occur which was more prominent at 80 °C. This investigation further suggests at lower temperature the tribofilm formed for PGZ lubricant should have thinner tribofilm for the same lubricant at 80 °C that results lower COF (Fig. 5(e)) but higher wear volume loss (Fig. 6(a)).

Fig. 17 shows the positive (*e, f*) and negative (*g, h*) ion spectra for PGZN0.05 wt% lubricant combination at 50 °C and 80 °C. Interestingly, the characteristics phosphate ion ($[PO_2]^-$ and $[PO_3]^-$) of ZDDP decomposition, were found in the negative ion spectra at 80 °C (in supplementary data *A2*). Conversely, at 50 °C these were not visible. Moreover, the metaphosphate ions are present in the 80 °C ion spectra but they are not apparently visible at 50 °C ion spectra. Presence of these ions shows

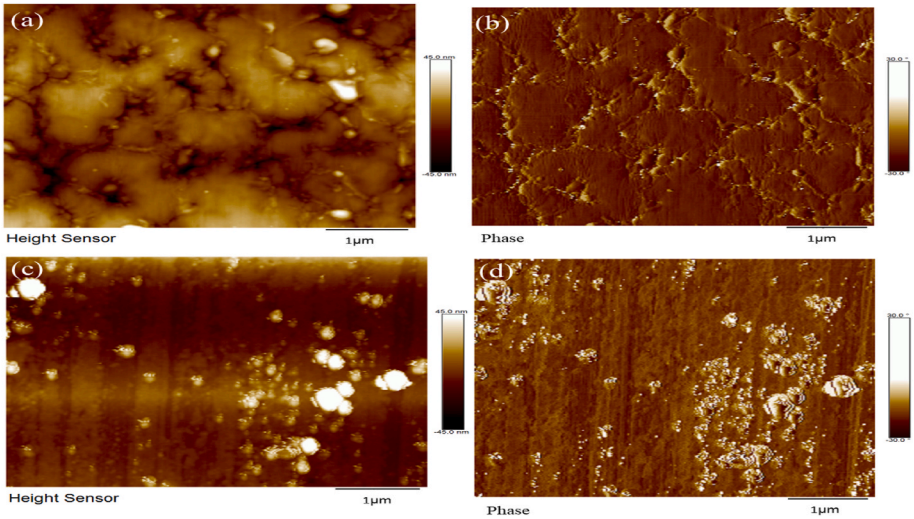

Fig. 15. Surface topography analysis by AFM for PGZ tribofilm (a) 2D height profile, (b) Phase profile and for PGZN0.05 wt% tribofilm (c) 2D height profile, (d) Phase profile. (A colour version of this figure can be viewed online.)

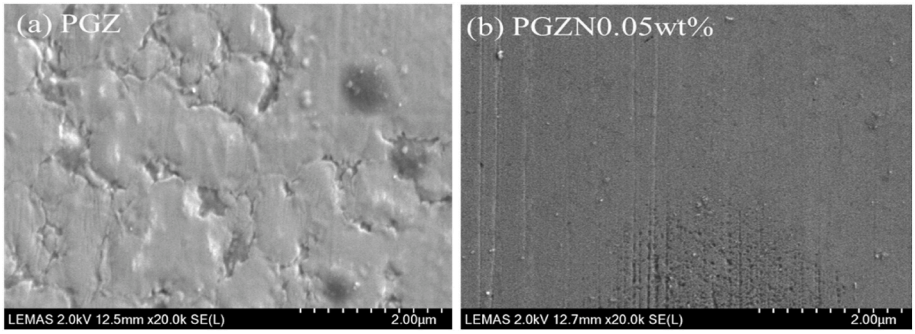

Fig. 16. Surface topography analysis of (a) PGZ and (b) PGZN0.05 wt% tribofilm formed at 80 °C by SEM.

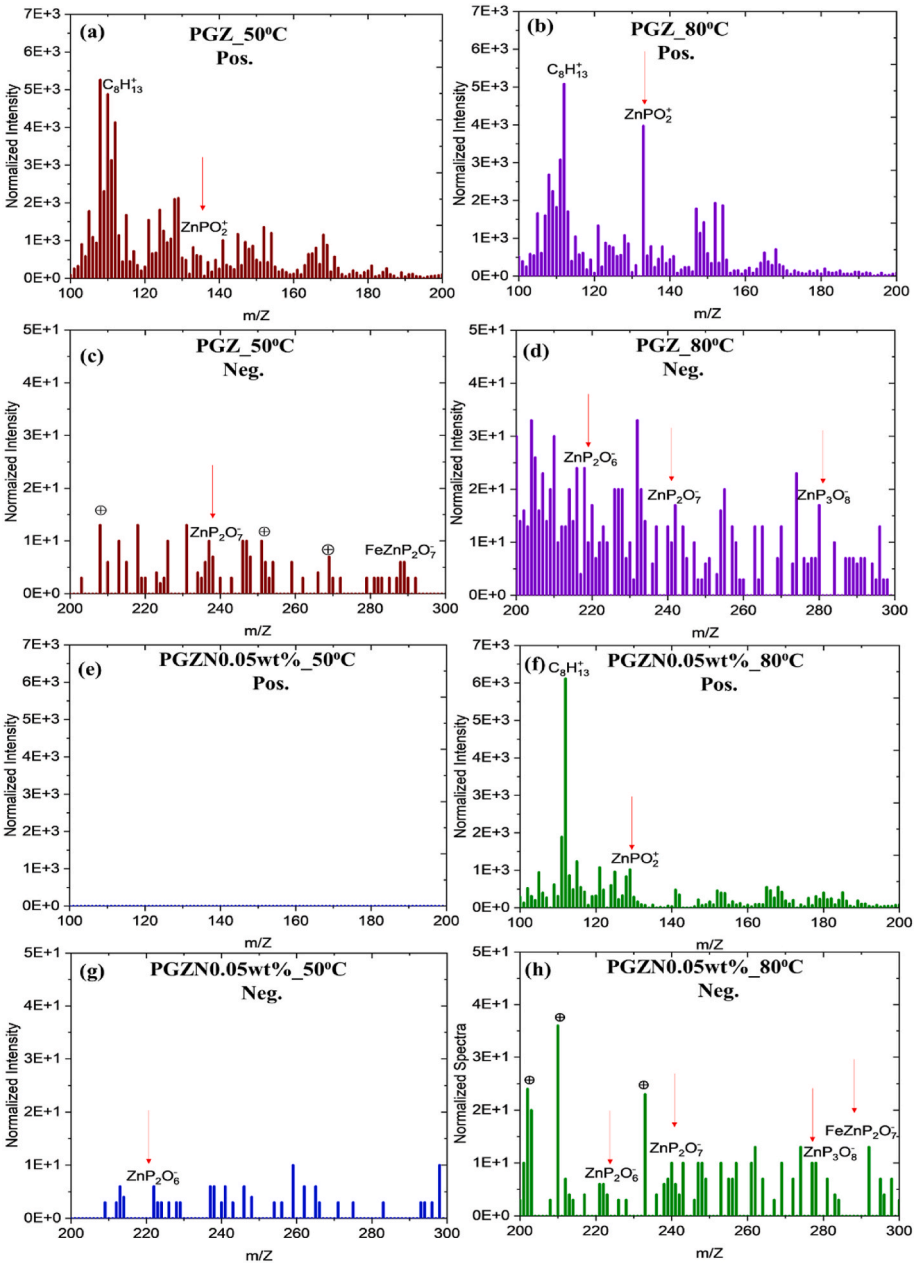

Fig. 17. Static SIMS ion spectra for PGZ lubricant derived tribofilm (a) positive ion spectra at 50 °C, (c) negative ion spectra at 50 °C, (b) positive ion spectra at 80 °C, (d) negative ion spectra at 80 °C and PGZN0.05 wt% lubricant derived tribofilm (e) positive ion spectra at 50 °C, (g) negative ion spectra at 50 °C, (f) positive ion spectra at 80 °C, (h) negative ion spectra at 80 °C (⊕ Characteristics peaks for the base oil). (A colour version of this figure can be viewed online.)

that addition of NDs in the lubricant combination did not hinder the GMO effect. Instead, it shows similar ion fragments like the PGZ lubricant combination. This phenomenon confirmed that temperature significantly affects GMO adsorption and ZDDP decomposition. Again, from the static SIMS analysis, the hydrocarbon moieties show the decomposition of GMO are not visible and one reason could be that PAO oil and GMO have similar structures making it difficult to distinguish. Another reason could be, in this work, only 1 wt% of GMO has been used and due to the bombardment of the surface, the primary ions broke the higher molecular fragments. Nevertheless, hydrocarbon moieties with the formulation of $[CnHm]^+$ are detected in the wear track that suggests GMO decomposition [14]. Addition of NDs in the lubricant combination, does not show significant modifications in the chemical structure even though HRTEM showed apparent changes in tribofilm thickness. The probable mechanism is discussed in the following section.

3.8. Lubrication mechanism

From Fig. 10, it is observed that the addition of NDs in the lubricant combination has significantly impacted the tribofilm thickness. Elemental analysis shows the presence of NDs inside the tribofilm that caused the difference. Schematic illustration of the lubrication mechanism is shown in Fig. 18 and explained in the following way:

1. Initially, in the binary additive system, the presence of GMO and ZDDP significantly altered the tribofilm formation (PGZ) at 80 °C temperature. GMO hinders the growth of ZDDP tribofilm and produces a considerably thin tribofilm (Fig. 10). In the boundary lubrication regime, this binary additive system showed a synergistic effect that reduced friction for lubricants without NDs. This is potentially due to the adsorption of GMO on the steel-contacting surface, which inhibits the growth of the ZDDP tribofilm [14]. This is in line with the hypothesis that GMO has an effect on restricting ZDDP tribofilm formation and decomposition, therefore adsorption of ZDDP can suppress on the surface depending on various temperatures [14,41].

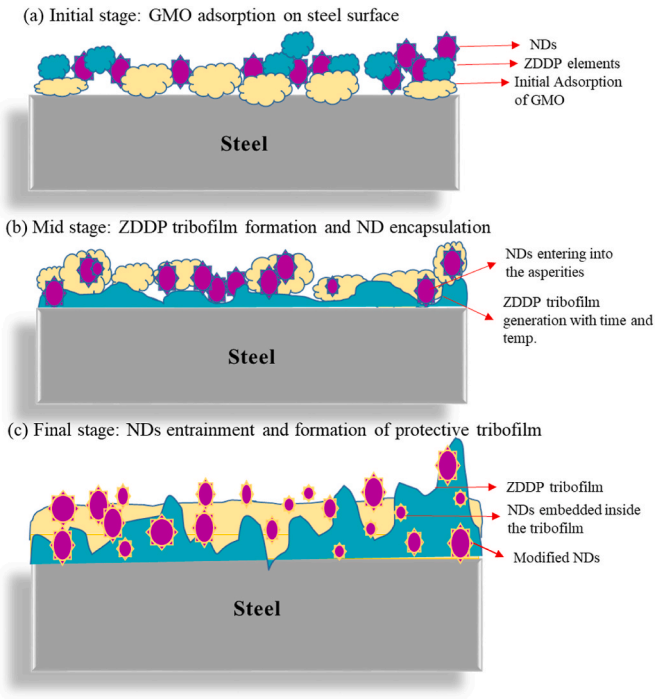

Fig. 18. Schematic illustration of friction reduction mechanism. (A colour version of this figure can be viewed online.)

2. As depicted, the picture that emerged from experimental and theoretical investigations yielded promising results for a lower coefficient of friction in the PGZN0.05 wt% lubricant combination:
   (a) Primarily, GMO was adsorbed on the steel surface which hinders the ZDDP tribofilm growth. Kano et al. confirmed that by tribochemical reaction on DLC surfaces, GMO decomposes into carboxylic acid [9]. These NDs were modified, and carboxylate functionalised. Again, it is proved that NDs have a structure similar to DLC coatings [68]. Hence, it can be hypothesised that GMO decomposed into carboxylic acid and encapsulates the carboxylated NDs by creating a protective layer around it.
   (b) With increased rubbing time and temperature, ZDDP decomposed into P and S rich layer and generated tribofilm.
   (c) While using base oil or lubricant combination with additives, NDs struggled to entrain into the asperity contacts due to mobility of oil. In this scenario, NDs settle down as sediments or move away from the contacting surfaces while maintaining movement in the oil flow. Either way, the movement of the NDs heavily depends on the bulk oil flow. During the time when NDs entrained into the asperity contact, the contacting surfaces were probably oxidised for both oil and ZDDP containing systems. This oxide or Zn, P, S rich layer acted as a matrix for NDs to roll into the asperity contact and embedded on the tribofilm layer [24]. Besides, NDs were almost spherical in shape and polished the sliding surface while rolling due to higher hardness [57]. Embedded NDs mechanically interlocked in the tribofilm and further retained the tribofilm on the sliding surfaces that stimulated continual surface protection that resulted in lower COF.

The shear properties of the formed tribofilm, reduce the resistance to motion by allowing smoother sliding between surfaces. From the Static SIMS analysis, it was found that tribofilm chemistry was similar with/without NDs, but the intensity of the ion fragments was changed due to the addition of NDs. The difference in frictional properties and shear strength was due to the presence of NDs in the lubricant combination.

4. Conclusion

In this study, a novel lubricant combination has been developed with PAO, GMO, low concentration ZDDP and ND combination. Frictional performance of newly developed nanolubricants was assessed at 50 °C and 80 °C. Lubricant combinations with NDs were found to be effective in friction and wear reduction at both temperatures. At boundary lubricating condition, PGZN0.05 wt% lubricant reduced the coefficient of friction by around 60 % and wear approximately 45 % when comparing with PAO oil at 80 °C. The main findings are:

a) Low concentration of carboxylated NDs (0.05 wt %) increases tribofilm thickness from 3-5 nm to 20–22 nm.
b) Temperature plays an integral role for the activation of the additives present in the lubricant combination. In this research, a new concept of lower concentration of ZDDP has been used and even with low concentration (0.2 wt%), ZDDP tribofilm is formed at higher temperature (80 °C), that worked as a matrix for the NDs to be mechanically interlocked, and hence increased the tribofilm thickness.
c) A new intriguing aspect, comprising the synergistic interaction between GMO and NDs has emerged from this systematic investigation. Adsorption of GMO on the steel surface and controlled decomposition of GMO further contributed to the encapsulation of NDs. These showed that the presence of GMO, and ND in the lubrication regime complemented the others and caused a substantial reduction in frictional properties.
d) Adsorption of GMO on steel surface, decomposition of GMO into carboxylic acid, encapsulation of NDs, mechanical interlocking of NDs into ZDDP tribofilm by rolling mechanism and finally polishing effect of NDs on the surfaces are the interrelated phenomena that

played pivotal role to reduce friction and wear for the newly developed nanolubricant.

The experimental findings presented demonstrate the potential to develop environmentally friendly low sulphated ash, Phosphorus, Sulphur (SAPS) lubricants by utilising ND/GMO/low concentration ZDDP synergy. Future work will focus on analysing the tribochemical interaction of carboxylated NDs and GMO by molecular dynamic simulation to verify the mechanism of the synergy observed.

CRediT authorship contribution statement

A.K. Piya: Conceptualization, Methodology, Investigation, Visualization, Software, Formal analysis, Writing – original draft. **L. Yang:** Investigation, Validation, Formal analysis, Supervision. **A. Al Sheikh Omar:** Writing – original draft, Writing – review & editing. **N. Emami:** Scientific input, Writing – review & editing, Supervision. **A. Morina:** Conceptualization, Scientific input, Writing – review & editing, Supervision, Project administration, Funding acquisition.

Declaration of competing interest

The authors declare that they have no known competing financial interests or personal relationships that could have appeared to influence the work reported in this paper.

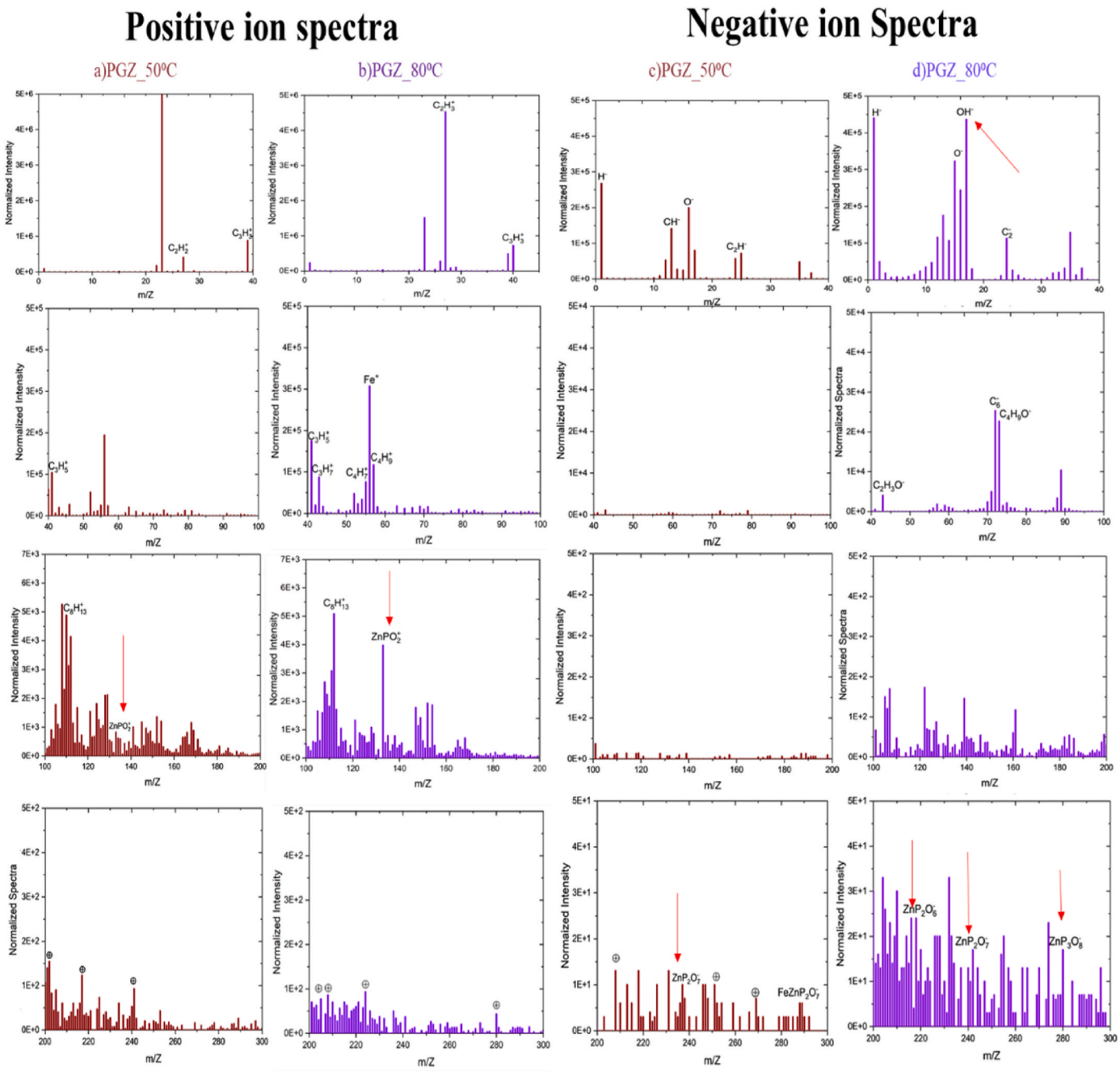

Fig. A1. Static SIMS ion spectra for PGZ lubricant derived tribofilm (a) Positive ion spectra at 50 °C (b) Positive ion spectra at 80 °C and (c) Negative ion spectra at 50 °C, (d) Negative ion spectra at 80 °C. (⊕ - peaks displayed by base oil).

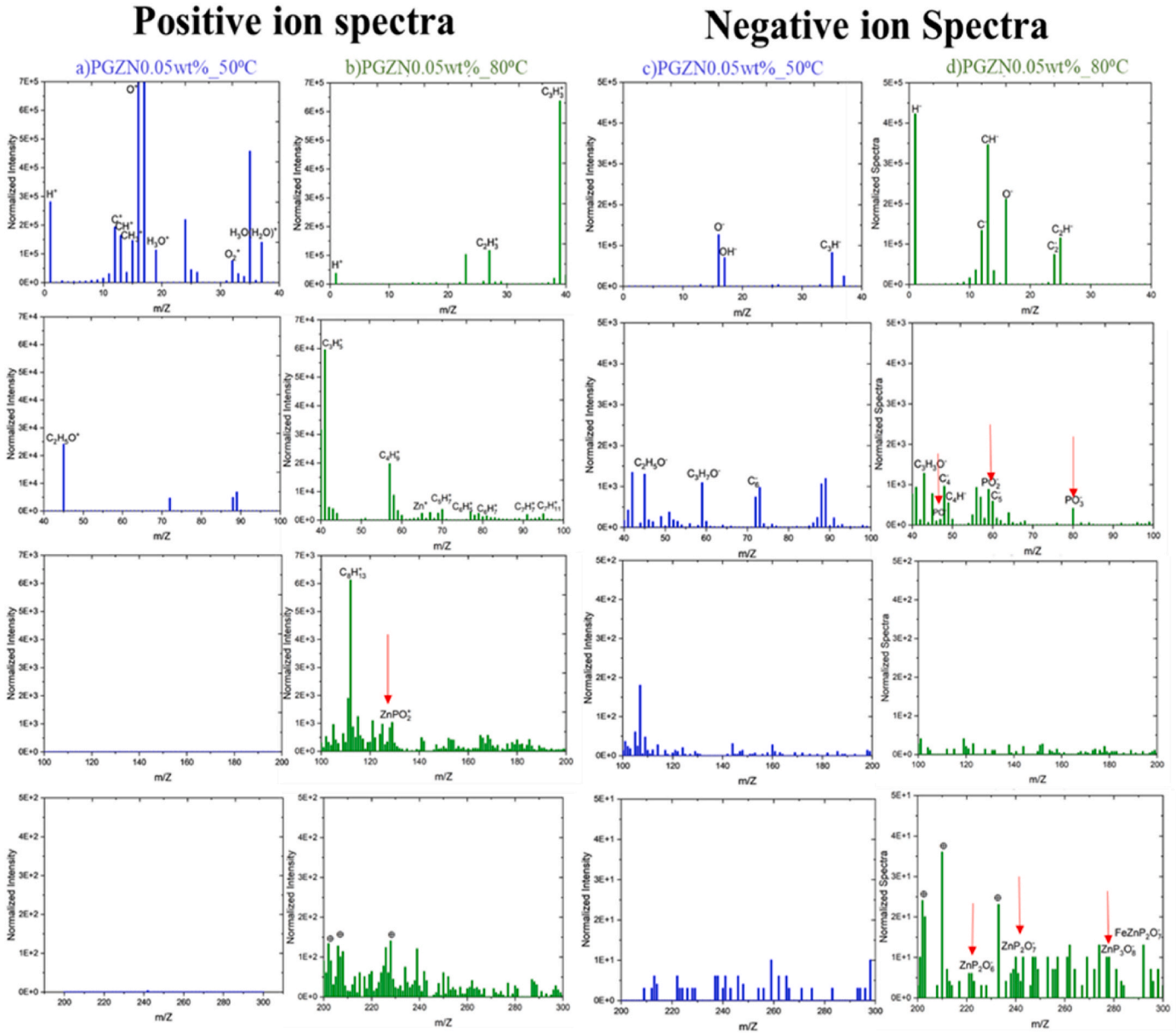

Fig. A2. Static SIMS ion spectra for PGZN0.05 wt% lubricant derived tribofilm (a) Positive ion spectra at 50 °C (b) Positive ion spectra at 80 °C and (c) Negative ion spectra at 50 °C, (d) Negative ion spectra at 80 °C. (◆ - peaks displayed by base oil).

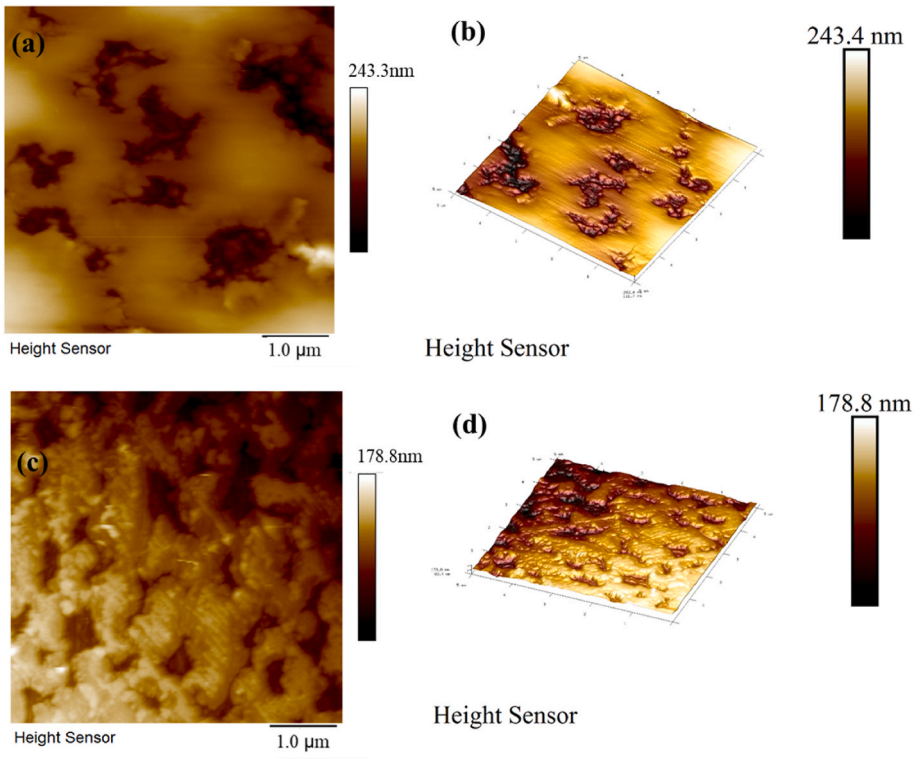

Fig. A3. PZ lubricated steel plate surface (a) 3D height profile, (b) 2D profile and PGZ lubricated steel plate surface (c) 3D height profile, (d) 2D profile, tested at 80 °C.

Acknowledgment

This project has received funding from the European Union's Horizon 2020 research and innovation programme under the Marie Skłodowska-Curie grant agreement No 860246. The authors also acknowledge the assistance of Dr.Chun Wang for AFM and Static SIMS measurement, Stuart Micklethwaite, Dr.Zabeada Aslam from LEMAS for FIB and HRTEM analysis and Mr. M M Raihan for reviewing and drafting the manuscript.

References

[1] K. Holmberg, P. Andersson, N.-O. Nylund, K. Mäkelä, A. Erdemir, Global energy consumption due to friction in trucks and buses, Tribol. Int. 78 (Oct. 2014) 94–114, https://doi.org/10.1016/j.triboint.2014.05.004.
[2] K. Holmberg, A. Erdemir, The impact of tribology on energy use and CO2 emission globally and in combustion engine and electric cars, Tribol. Int. 135 (Jul. 2019) 389–396, https://doi.org/10.1016/j.triboint.2019.03.024.
[3] S. Gupta, M. Zaid, A. Kumar, Y. Singh, Effect of Jojoba oil based biolubricant additive on the friction and wear characteristics of the Al-7Si alloy, Mater. Today Proc. 26 (Jan. 2020) 2681–2684, https://doi.org/10.1016/j.matpr.2020.02.564.
[4] C.-J. Hsu, A. Stratmann, A. Rosenkranz, C. Gachot, Enhanced growth of ZDDP-based tribofilms on laser-interference patterned cylinder roller bearings, Lubricants 5 (4) (Dec. 2017), https://doi.org/10.3390/lubricants5040039. Art. no. 4.
[5] D. She, et al., Friction-reduction and anti-wear properties of polyalphaolefin oil with Mo-DTC additive enhanced by nano-carbon materials, Appl. Nanosci. 10 (9) (Sep. 2020) 3539–3551, https://doi.org/10.1007/s13204-020-01458-z.
[6] H. Spikes, Friction modifier additives, Tribol. Lett. 60 (1) (Sep. 2015) 5, https://doi.org/10.1007/s11249-015-0589-z.
[7] H. Okubo, C. Tadokoro, S. Sasaki, Tribological properties of a tetrahedral amorphous carbon (ta-C) film under boundary lubrication in the presence of organic friction modifiers and zinc dialkyldithiophosphate (ZDDP), Wear 332 (333) (May 2015) 1293–1302, https://doi.org/10.1016/j.wear.2015.01.023.
[8] M. Ratoi, V.B. Niste, H. Alghawel, Y.F. Suen, K. Nelson, The impact of organic friction modifiers on engine oil tribofilms, RSC Adv. 4 (9) (Dec. 2013) 4278–4285, https://doi.org/10.1039/C3RA46403B.
[9] M. Kano, et al., Ultralow friction of DLC in presence of glycerol mono-oleate (GNO), Tribol. Lett. 18 (2) (Feb. 2005) 245–251, https://doi.org/10.1007/s11249-004-2749-4.
[10] J.U. Dawczyk, The Effect of Organic Friction Modifiers on ZDDP Tribofilm, Apr. 2018, https://doi.org/10.25560/72903.
[11] S. Yazawa, I. Minami, B. Prakash, Reducing friction and wear of tribological systems through hybrid tribofilm consisting of coating and lubricants, Lubricants 2 (2) (Jun. 2014), https://doi.org/10.3390/lubricants2020090. Art. no. 2.
[12] L.J. Taylor, H.A. Spikes, Friction-enhancing properties of ZDDP antiwear additive: Part I—friction and morphology of ZDDP reaction films, Tribol. Trans. 46 (3) (Jan. 2003) 303–309, https://doi.org/10.1080/10402000308982630.
[13] H. Okubo, S. Watanabe, C. Tadokoro, S. Sasaki, Effects of concentration of zinc dialkyldithiophosphate on the tribological properties of tetrahedral amorphous carbon films in presence of organic friction modifiers, Tribol. Int. 94 (Feb. 2016) 446–457, https://doi.org/10.1016/j.triboint.2015.10.008.
[14] F. Cyriac, T. X. Yi, S. K. Poornachary, and P. S. Chow, "Effect of temperature on tribological performance of organic friction modifier and anti-wear additive: insights from friction, surface (ToF-SIMS and EDX) and wear analysis," Tribol. Int., vol. 157, 637554240000000000, doi: 10.1016/j.triboint.2021.106896.
[15] D. Kim, T.J. Toops, K. Nguyen, M.J. Lance, J. Qu, Impact of primary and secondary ZDDP and ionic liquid as lubricant oil additives on the performance and physicochemical properties of Pd-based three-way catalysts, Catalysts 11 (8) (Aug. 2021), https://doi.org/10.3390/catal11080878. Art. no. 8.
[16] M. Ivanov, O. Shenderova, Nanodiamond-based nanolubricants for motor oils, Curr. Opin. Solid State Mater. Sci. 21 (1) (Feb. 2017) 17–24, https://doi.org/10.1016/j.cossms.2016.07.003.
[17] X. Tao, Z. Jiazheng, X. Kang, The ball-bearing effect of diamond nanoparticles as an oil additive, J. Phys. Appl. Phys. 29 (11) (Nov. 1996) 2932, https://doi.org/10.1088/0022-3727/29/11/029.
[18] M. Marko, J. Kyle, B. Branson, E. Terrell, Tribological improvements of dispersed nanodiamond additives in lubricating mineral oil, J. Tribol. 137 (1) (Oct. 2014), https://doi.org/10.1115/1.4028554.
[19] B. Acharya, K.S. Avva, B. Thapa, T.N. Pardue, J. Krim, Synergistic effect of nanodiamond and phosphate ester anti-wear additive blends, Lubricants 6 (2) (Jun. 2018), https://doi.org/10.3390/lubricants6020056. Art. no. 2.
[20] A. Golchin, A. Villain, N. Emami, Tribological behaviour of nanodiamond reinforced UHMWPE in water-lubricated contacts, Tribol. Int. 110 (Jan. 2017), https://doi.org/10.1016/j.triboint.2017.01.016.
[21] M. Ivanov, O. Shenderova, Nanodiamond-based nanolubricants for motor oils, Curr. Opin. Solid State Mater. Sci. 21 (1) (Feb. 2017) 17–24, https://doi.org/10.1016/j.cossms.2016.07.003.
[22] Y. Liu, S. Yu, W. Wang, Nanodiamond plates as macroscale solid lubricant: a 'non-layered' two-dimension material, Carbon 198 (Oct. 2022) 119–131, https://doi.org/10.1016/j.carbon.2022.07.006.
[23] S. Yu, et al., Lubrication and anti-wear behavior of duplex annealed nanodiamonds/PEO coating on Ti6Al4V: functional mechanism of structural transformation, Surf. Coat. Technol. 461 (May 2023), 129426, https://doi.org/10.1016/j.surfcoat.2023.129426.
[24] B. Acharya, C.M. Seed, J. Krim, Shear activation of ZDDP reaction films in the presence and absence of nanodiamonds, Appl. Surf. Sci. Adv. 7 (Feb. 2022), 100214, https://doi.org/10.1016/j.apsadv.2022.100214.

[25] A. Khajeh, J. Krim, A. Martini, Synergistic effect of nanodiamonds on the adsorption of tricresyl phosphate on iron oxide surfaces, Appl. Phys. Lett. 114 (17) (Apr. 2019), 171602, https://doi.org/10.1063/1.5093425.

[26] G.-J. Lee, J.-J. Park, M.-K. Lee, C.K. Rhee, Stable dispersion of nanodiamonds in oil and their tribological properties as lubricant additives, Appl. Surf. Sci. 415 (Sep. 2017) 24–27, https://doi.org/10.1016/j.apsusc.2016.12.109.

[27] M. Ivanov, O. Shenderova, Nanodiamond-based nanolubricants for motor oils, Curr. Opin. Solid State Mater. Sci. 21 (1) (Feb. 2017) 17–24, https://doi.org/10.1016/j.cossms.2016.07.003.

[28] S.M. Alves, V.S. Mello, E.A. Faria, A.P.P. Camargo, Nanolubricants developed from tiny CuO nanoparticles, Tribol. Int. 100 (Aug. 2016) 263–271, https://doi.org/10.1016/j.triboint.2016.01.050.

[29] D.G. Lim, et al., Comprehensive evaluation of carboxylated nanodiamond as a topical drug delivery system, Int. J. Nanomed. 11 (2016) 2381–2395, https://doi.org/10.2147/IJN.S104859.

[30] J.J. Truhan, J. Qu, P.J. Blau, A rig test to measure friction and wear of heavy duty diesel engine piston rings and cylinder liners using realistic lubricants, Tribol. Int. 38 (3) (Mar. 2005) 211–218, https://doi.org/10.1016/j.triboint.2004.08.003.

[31] A. Al Sheikh Omar, F. Motamen Salehi, U. Farooq, A. Morina, A. Neville, Chemical and physical assessment of engine oils degradation and additive depletion by soot, Tribol. Int. 160 (Aug. 2021), 107054, https://doi.org/10.1016/j.triboint.2021.107054.

[32] B.J. Hamrock, D. Dowson, Isothermal elastohydrodynamic lubrication of point contacts: Part III—fully flooded results, J. Lubr. Technol. 99 (2) (Apr. 1977) 264–275, https://doi.org/10.1115/1.3453074.

[33] D. Wang, C. Song, Y. Shao, S. Song, S. Peng, F. Xiao, Optimal control strategy for series hybrid electric vehicles in the warm-up process, Energies 11 (5) (May 2018), https://doi.org/10.3390/en11051091. Art. no. 5.

[34] S.V. Baryshev, R.A. Erck, J.F. Moore, A.V. Zinovev, C.E. Tripa, I.V. Veryovkin, Characterization of surface modifications by white light interferometry: applications in ion sputtering, laser ablation, and tribology experiments, J. Vis. Exp. 72 (Feb. 2013), 50260, https://doi.org/10.3791/50260.

[35] D. Xu, C. Wang, C. Espejo, J. Wang, A. Neville, A. Morina, Understanding the friction reduction mechanism based on molybdenum disulfide tribofilm formation and removal, Langmuir 34 (45) (Nov. 2018) 13523–13533, https://doi.org/10.1021/acs.langmuir.8b02329.

[36] M.A. Ashraf, W. Peng, Y. Zare, K.Y. Rhee, Effects of size and aggregation/agglomeration of nanoparticles on the interfacial/interphase properties and tensile strength of polymer nanocomposites, Nanoscale Res. Lett. 13 (1) (Dec. 2018) 214, https://doi.org/10.1186/s11671-018-2624-0.

[37] T. Petit, L. Puskar, FTIR spectroscopy of nanodiamonds: methods and interpretation, Diam. Relat. Mater. 89 (Oct. 2018) 52–66, https://doi.org/10.1016/j.diamond.2018.08.005.

[38] G. Caron, G. Ermondi, R.A. Scherrer, 5.18 - lipophilicity, polarity, and hydrophobicity, in: J.B. Taylor, D.J. Triggle (Eds.), Comprehensive Medicinal Chemistry II, Elsevier, Oxford, 2007, pp. 425–452, https://doi.org/10.1016/B0-08-045044-X/00135-8.

[39] Y. Zare, Study of nanoparticles aggregation/agglomeration in polymer particulate nanocomposites by mechanical properties, Compos. Part Appl. Sci. Manuf. 84 (May 2016) 158–164, https://doi.org/10.1016/j.compositesa.2016.01.020.

[40] W. Wang, B. Shen, Y. Li, Q. Ni, L. Zhou, F. Du, Friction reduction mechanism of glycerol monooleate-containing lubricants at elevated temperature - transition from physisorption to chemisorption, Sci. Prog. 104 (1) (Jan. 2021), 0036850421998529, https://doi.org/10.1177/0036850421998529.

[41] F. Cyriac, T.X. Yi, S.K. Poornachary, P.S. Chow, Influence of base oil polarity on the tribological performance of surface-active engine oil additives, Tribol. Lett. 69 (3) (Jun. 2021) 87, https://doi.org/10.1007/s11249-021-01463-5.

[42] A. Morina, A. Neville, M. Priest, J.H. Green, ZDDP and MoDTC interactions in boundary lubrication—the effect of temperature and ZDDP/MoDTC ratio, Tribol. Int. 39 (12) (Dec. 2006) 1545–1557, https://doi.org/10.1016/j.triboint.2006.03.001.

[43] K.T. Miklozic, T.R. Forbus, H.A. Spikes, Performance of friction modifiers on ZDDP-generated surfaces, Tribol. Trans. 50 (3) (Jun. 2007) 328–335, https://doi.org/10.1080/10402000701413505.

[44] H. Spikes, The history and mechanisms of ZDDP, Tribol. Lett. 17 (3) (Oct. 2004) 469–489, https://doi.org/10.1023/B:TRIL.0000044495.26882.b5.

[45] W. Wang, B. Shen, Y. Li, Q. Ni, L. Zhou, F. Du, Friction reduction mechanism of glycerol monooleate-containing lubricants at elevated temperature - transition from physisorption to chemisorption, Sci. Prog. 104 (1) (Jan. 2021), 0036850421998529, https://doi.org/10.1177/0036850421998529.

[46] S.-W. Hwang, S.-C. Chang, T. Zhang, H.-K. Kim, Tribology behavior of a lubricant with nano-diamond particles on steel, Int. J. Eng. Technol. 9 (1) (Feb. 2017) 169–174, https://doi.org/10.21817/ijet/2017/v9i1/170901417.

[47] B. Acharya, T.N. Pardue, K.S. Avva, J. Krim, In situ, real time studies of thermal reaction film formation temperatures for iron and 304SS surfaces immersed in 5% tricresyl phosphate in base oil, Tribol. Int. 126 (Oct. 2018) 106–115, https://doi.org/10.1016/j.triboint.2018.04.034.

[48] A. Morina, A. Neville, M. Priest, J.H. Green, ZDDP and MoDTC interactions in boundary lubrication—the effect of temperature and ZDDP/MoDTC ratio, Tribol. Int. 39 (12) (Dec. 2006) 1545–1557, https://doi.org/10.1016/j.triboint.2006.03.001.

[49] J.F. Luiz, H. Spikes, Tribofilm Formation, friction and wear-reducing properties of some phosphorus-containing antiwear additives, Tribol. Lett. 68 (3) (Jul. 2020) 75, https://doi.org/10.1007/s11249-020-01315-8.

[50] J.M. Martin, Antiwear mechanisms of zinc dithiophosphate: a chemical hardness approach, Tribol. Lett. 6 (1) (Jan. 1999) 1–8, https://doi.org/10.1023/A:1019191019134.

[51] Y. Pei, D. Xia, S. Wang, L. Cong, X. Wang, D. Wang, Effects of temperature on the tribological properties of NM600 under sliding wear, Materials 12 (23) (Dec. 2019) 4009, https://doi.org/10.3390/ma12234009.

[52] H. Spikes, The history and mechanisms of ZDDP, Tribol. Lett. 17 (3) (Oct. 2004) 469–489, https://doi.org/10.1023/B:TRIL.0000044495.26882.b5.

[53] A. Morina, A. Neville, M. Priest, J.H. Green, ZDDP and MoDTC interactions in boundary lubrication—the effect of temperature and ZDDP/MoDTC ratio, Tribol. Int. 39 (12) (Dec. 2006) 1545–1557, https://doi.org/10.1016/j.triboint.2006.03.001.

[54] A. Raina, et al., Nanodiamond particles as secondary additive for polyalphaolefin oil lubrication of steel-aluminium contact, Nanomater. Basel Switz. 11 (6) (May 2021) 1438, https://doi.org/10.3390/nano11061438.

[55] A. Raina, A. Anand, Effect of nanodiamond on friction and wear behavior of metal dichalcogenides in synthetic oil, Appl. Nanosci. 8 (4) (Apr. 2018) 581–591, https://doi.org/10.1007/s13204-018-0695-y.

[56] A. Raina, A. Anand, Tribological investigation of diamond nanoparticles for steel/steel contacts in boundary lubrication regime, Appl. Nanosci. 7 (7) (Oct. 2017) 371–388, https://doi.org/10.1007/s13204-017-0590-y.

[57] W. Zhai, W. Lu, X. Liu, L. Zhou, Nanodiamond as an effective additive in oil to dramatically reduce friction and wear for fretting steel/copper interfaces, Tribol. Int. 129 (Jan. 2019) 75–81, https://doi.org/10.1016/j.triboint.2018.08.006.

[58] A. Afandi, A. Howkins, I.W. Boyd, R.B. Jackman, Nanodiamonds for device applications: an investigation of the properties of boron-doped detonation nanodiamonds, Sci. Rep. 8 (Feb. 2018) 3270, https://doi.org/10.1038/s41598-018-21670-w.

[59] K.T. Miklozic, T.R. Forbus, H.A. Spikes, Performance of friction modifiers on ZDDP-generated surfaces, Tribol. Trans. 50 (3) (Jun. 2007) 328–335, https://doi.org/10.1080/10402000701413505.

[60] E. Oblak, M. Kalin, Relationship between the nanoscale topographical and mechanical properties of tribochemical films on DLC coatings and their macroscopic friction behavior, Tribol. Lett. 59 (3) (Aug. 2015) 49, https://doi.org/10.1007/s11249-015-0575-5.

[61] A. Tomala, A. Naveira-Suarez, I.C. Gebeshuber, R. Pasaribu, Effect of base oil polarity on micro and nanofriction behaviour of base oil + ZDDP solutions, Tribol. Mater. Surface Interfac. 3 (4) (Dec. 2009) 182–188, https://doi.org/10.1179/175158310X481709.

[62] K. Sato, S. Watanabe, S. Sasaki, High friction mechanism of ZDDP tribofilm based on in situ AFM observation of nano-friction and adhesion properties, Tribol. Lett. 70 (3) (Aug. 2022) 94, https://doi.org/10.1007/s11249-022-01635-x.

[63] S. Oras, S. Vlassov, M. Berholts, R. Lõhmus, K. Mougin, Tuning adhesion forces between functionalized gold colloidal nanoparticles and silicon AFM tips: role of ligands and capillary forces, Beilstein J. Nanotechnol. 9 (1) (Feb. 2018) 660–670, https://doi.org/10.3762/bjnano.9.61.

[64] R. Dong, L.E. Yu, Investigation of surface changes of nanoparticles using TM-AFM phase imaging, Environ. Sci. Technol. 37 (12) (Jun. 2003) 2813–2819, https://doi.org/10.1021/es034071k.

[65] O. Marti, Measurement of adhesion and pull-off forces with the AFM, vol. 5, in Mechanics & Materials Science, in: Modern Tribology Handbook, Two Volume Set, 5, 2000, https://doi.org/10.1201/9780849377877.ch17. CRC Press.

[66] J. Tamayo, R. García, Deformation, contact time, and phase contrast in tapping mode scanning force microscopy, Langmuir 12 (18) (Jan. 1996) 4430–4435, https://doi.org/10.1021/la960189l.

[67] S.N. Magonov, V. Elings, M.-H. Whangbo, Phase imaging and stiffness in tapping-mode atomic force microscopy, Surf. Sci. 375 (2) (Apr. 1997) L385–L391, https://doi.org/10.1016/S0039-6028(96)01591-9.

[68] A. Raina, A. Anand, Tribological investigation of diamond nanoparticles for steel/steel contacts in boundary lubrication regime, Appl. Nanosci. 7 (7) (Oct. 2017) 371–388, https://doi.org/10.1007/s13204-017-0590-y.

[69] C. Minfray, J.M. Martin, M.I. De Barros, T.L. Mogne, R. Kersting, B. Hagenhoff, Chemistry of ZDDP tribofilm by ToF-SIMS, Tribol. Lett. 17 (3) (Oct. 2004) 351–357, https://doi.org/10.1023/B:TRIL.0000044483.68571.49.

[70] S. Jiang, C. Yuan, J.S.S. Wong, Effectiveness of glycerol-monooleate in high-performance polymer tribo-systems, Tribol. Int. 155 (Mar. 2021), 106753, https://doi.org/10.1016/j.triboint.2020.106753.

[71] J.L. Bradley-Shaw, P.J. Camp, P.J. Dowding, K. Lewtas, Self-assembly and friction of glycerol monooleate and its hydrolysis products in bulk and confined non-aqueous solvents, Phys. Chem. Chem. Phys. 20 (26) (Jul. 2018) 17648–17657, https://doi.org/10.1039/C8CP01785A.

[72] L.J. Taylor, H.A. Spikes, Friction-enhancing properties of ZDDP antiwear additive: Part I—friction and morphology of ZDDP reaction films, Tribol. Trans. 46 (3) (Jan. 2003) 303–309, https://doi.org/10.1080/10402000308982630.

[73] A. Morina, A. Neville, Tribofilms: aspects of formation, stability and removal, J. Phys. Appl. Phys. 40 (18) (Sep. 2007) 5476–5487, https://doi.org/10.1088/0022-3727/40/18/S08.